25. Precise Point Positioning

Jan Kouba, François Lahaye, Pierre Tétreault

Since its introduction in 1997, precise point positioning (PPP) offers an attractive alternative to differential global navigation satellite system (GNSS) positioning. The PPP approach uses undifferenced, dual-frequency, pseudorange and carrier-phase observations along with precise satellite orbit and clock products, for standalone static or kinematic geodetic point positioning with centimeter precision. This chapter introduces the PPP concept and specifies the required models needed to correct for systematic effects causing centimeter-level variations in the satellite-to-user range. For completeness, models and methods for processing single-frequency GNSS data are presented and specific aspects of GLONASS (Global'naya Navigatsionnaya Sputnikova Sistema) and new GNSSs are also described. Furthermore, recent developments in fixing undifferenced carrier-phase ambiguities, which can considerably shorten or nearly eliminate the initial delay for PPP convergence, are highlighted. Existing web applications and real-time corrections services enabling post-mission and real-time PPP are presented. Finally, typical PPP precision and accuracy estimates are discussed, including the solution of station tropospheric zenith path delays and receiver clocks, with millimeter and nanosecond precision respectively.

The potential of GNSS for geodetic positioning applications was realized quite early during the Global Positioning System (GPS) implementation stage [25.1]. A relative positioning method, utilizing carrier-phase measurements made simultaneously and doubly differenced (DD) between two observing stations and two satellites, was proposed to eliminate the satellite and receiver clock offsets. Until the mid-1990s, practically all geodetic GPS applications employed relative baseline positioning with DD carrier-phase observations (Chap. 26).

In 1997, a new approach called precise point positioning (PPP), utilizing undifferenced carrier-phase and pseudorange observations was introduced by *Zumberge* et al. [25.2]. Unlike the traditional DD relative baseline positioning, PPP does not require simultaneous observations at two stations. PPP, in fact, is a logical extension of the GNSS pseudorange navigation, which replaces the broadcast satellite orbits and clocks with precise estimates, and includes the precise carrier-phase observations in addition to the pseudoranges. This, however, necessitates the introduction of additional initial phase ambiguity unknowns, causing a fairly long (up to 15 min or longer) initial convergence of PPP solutions. It also entails careful modeling and data screening for outliers and carrier-phase cycle

slips, which is more challenging than for the DD approach.

PPP also requires much more careful modeling of local station and environmental effects than DD relative positioning. However, in addition to precise position solutions, PPP provides precise station clocks and tropospheric zenith path delays (ZTDs), which are either unavailable or less precise in the case of DD positioning. The greater availability of precise orbit and clock solution products in late 1990s, thanks in great part to the organized efforts of the International GNSS Service (IGS); (Chap. 33), increased the popularity of PPP for geodetic and many other applications, for example in geodynamics, meteorology, metrology [25.3] and so on. This is clearly demonstrated by the popularity of the several online PPP services and PPP software packages now available.

The purpose of this chapter is to provide an overview of the PPP concept, state-of-the art PPP modeling techniques and the achievable performances. In Sect. 25.1 the PPP concept is introduced, followed by Sect. 25.2, which discusses conventional correction models and compatibility aspects. This is complemented by a review of specific processing aspects such as single-frequency and multi-GNSS PPP as well as the recent developments of precise point positioning using undifferenced phase ambiguity fixing (Sect. 25.3). The last two sections, 25.4 and 25.5, respectively list available PPP implementations and services and provide more detailed examples of recent PPP results.

25.1 PPP Concept

The PPP approach assumes that globally consistent satellite orbits and clocks are fixed or heavily constrained, and that PPP mathematical models are consistent with those applied in the global network solutions from which the orbit/clock products were estimated. In general, this consistency can be readily achieved if both the global orbit/clock and PPP solutions adhere to the same international standards, such as the current International Earth Rotation and Reference Systems Service (IERS) conventions. Since carrier-phase observations are used, PPP must estimate initial phase ambiguities to all satellites, in addition to the station position, station clock offsets and tropospheric zenith path delays (ZTD). The PPP method can be conceptualized as a back substitution of single station data into a global solution condensed in the form of the global satellite orbits and clocks and associated conventions and standards. Although PPP itself uses data from a single station only, computation of the satellite orbits and clocks needed for its implementation require the use of a global tracking network.

25.1.1 Observation Equations

For PPP, typically dual-frequency data is combined in order to eliminate nearly all of the ionospheric propagation delays. The ionosphere-free (IF) combinations (Chap. 19) of dual-frequency GNSS pseudorange (p_{IF}) and carrier-phase observations (φ_{IF}) are related to the user position, clock, troposphere and ambiguity parameters according to the following simplified observation equations (Chap. 19)

$$\begin{aligned} p^{\mathrm{s}}_{\mathrm{r,IF}} &= \rho^{\mathrm{s}}_{\mathrm{r}} + c\,(dt_{\mathrm{r}} - dt^{\mathrm{s}}) + T^{\mathrm{s}}_{\mathrm{r}} + e_{\mathrm{IF}}\,, \\ \varphi^{\mathrm{s}}_{\mathrm{r,IF}} &= \rho^{\mathrm{s}}_{\mathrm{r}} + c\,(dt_{\mathrm{r}} - dt^{\mathrm{s}}) + T^{\mathrm{s}}_{\mathrm{r}} + \lambda_{\mathrm{IF}} A_{\mathrm{IF}} + \epsilon_{\mathrm{IF}}\,, \end{aligned} \quad (25.1)$$

where:

- $p^{\mathrm{s}}_{\mathrm{r,IF}}$ is the ionosphere-free combination $(f_{\mathrm{A}}^2 p_{\mathrm{A}} - f_{\mathrm{B}}^2 p_{\mathrm{B}})/(f_{\mathrm{A}}^2 - f_{\mathrm{B}}^2)$ of pseudoranges p_{A} and p_{B} observed at two distinct signal frequencies f_{A} and f_{B}.
- $\varphi^{\mathrm{s}}_{\mathrm{r,IF}}$ is the ionosphere-free combination $(f_{\mathrm{A}}^2 \varphi_{\mathrm{A}} - f_{\mathrm{B}}^2 \varphi_{\mathrm{B}})/(f_{\mathrm{A}}^2 - f_{\mathrm{B}}^2)$ of the corresponding carrier-phases φ_{A} and φ_{B}.
- $\rho^{\mathrm{s}}_{\mathrm{r}}$ is the geometrical range $||\boldsymbol{x}^{\mathrm{s}} - \boldsymbol{x}_{\mathrm{r}}||$ from the satellite position $\boldsymbol{x}^{\mathrm{s}} = (x^{\mathrm{s}}, y^{\mathrm{s}}, z^{\mathrm{s}})^{\top}$ at the signal emission epoch t_{E} to the receiver position $\boldsymbol{x}_{\mathrm{r}} = (x_{\mathrm{r}}, y_{\mathrm{r}}, z_{\mathrm{r}})^{\top}$ at its reception (arrival) epoch $t_{\mathrm{A}} \cong t_{\mathrm{E}} + \rho^{\mathrm{s}}_{\mathrm{r}}/c$.
- dt_{r} is the receiver clock offset from the GNSS time (including receiver code biases and delays).
- dt^{s} is the satellite clock offset from the GNSS system time (including satellite code biases and delays).
- c is the vacuum speed of light.
- $T^{\mathrm{s}}_{\mathrm{r}}$ is the signal path delay due to the neutral atmosphere (primarily the troposphere).
- A_{IF} is the *noninteger* ambiguity of the IF carrier-phase combination, actually the IF combination of the φ_{A} and φ_{B} integer ambiguities and noninteger initial phase delays.
- λ_{IF} is the IF combination of the carrier-phase wavelengths λ_{A} and λ_{B} of signals A and B (e.g., 10.7 cm for GPS L1 and L2).
- $e_{\mathrm{IF}}, \epsilon_{\mathrm{IF}}$ are the relevant measurement noise components, including multipath of the IF pseudorange and carrier-phase combinations.

Since the global GNSS orbit/clock parameters are held fixed, the satellite coordinates $(x^{\mathrm{s}}, y^{\mathrm{s}}, z^{\mathrm{s}})$ and the satellite clocks dt^{s} in (25.1) are considered known.

Furthermore, the unknown wet part of the tropospheric delay is usually expressed as a product of the wet zenith tropospheric delay ZTD_w and a mapping function that relates the slant wet delay to the zenith delay. As a result, the unknown parameters of a typical PPP model are: receiver position coordinates (x_r, y_r, z_r), receiver clock (dt_r), zenith troposphere delay (ZTD_w) and (noninteger) IF carrier-phase ambiguities (A_{IF}).

After fixing the known satellite clocks and positions, the above observation equations contain observations and unknowns pertaining to a single station only. Note that satellite clock and orbit weighting does not require the satellite clock and position parameterizations, since they can be effectively accounted for by satellite-specific pseudorange/phase observation weighting. When fixing orbits/clocks, it makes little or no sense to solve (25.1) in a network solution, as it would still result in uncorrelated station solutions that are exactly identical to independent, single station, PPP solutions. Also note that, unlike relative or network solutions utilizing DD phase observations, it is not possible to fix individual integer ambiguities for the two signals A and B in single point positioning solutions without additional parameterization of measurement biases (Sect. 25.3.4).

It is worth noting that PPP provides position, ZTD and receiver-clock estimates that are consistent with the global reference system implied by the fixed global GNSS orbit/clock solutions. The DD approach, on the other hand, does not offer any clock solutions, and the ZTD solutions may be biased by a constant (datum) offset, in particular for regional or local network, or single baseline (< 500 km) solutions. This ZTD bias, in turn, may cause a small-scale error in relative height solutions. Thus, such regional or local ZTD solutions, based on DD analyses, require external tropospheric ZTD calibration (at least at one station of the network), for example by means of the IGS tropospheric combined ZTD products (Chaps. 38 and 33).

Traditionally, GPS L1 and L2 observation pairs have been used in PPP applications in view of the availability of highest precision orbit and clock products compatible with these signals. However, some GNSS, like the emerging Galileo or the modernized GPS systems, may also provide E5 or L5 carrier-phase observations instead of, or in addition to, those on the L2 frequency. The above dual-frequency PPP discussion is generically valid for any pair of (sufficiently spaced) signal frequencies f_A and f_B. The possible use and impact of three frequency observations, which are also becoming available for new or modernized GNSSs, are briefly discussed below in Sects. 25.2.1 and 25.3.4.

25.1.2 Adjustment and Quality Control

The design matrix needed for the adjustment follows from a linearization of the observation equations around the approximate parameter values (Chap. 21). It consists of the partial derivatives of (25.1) with respect to the four types of PPP parameters: station position, receiver clock, zenith troposphere delay, and (noninteger) IF carrier-phase ambiguities.

Batch versus Sequential

The adjustment can be done in a single step, the so-called batch adjustment (with iterations), or alternatively within a sequential adjustment or filter (with or without iterations) that can be adapted to varying user dynamics (Chap. 22). The disadvantage of a batch adjustment is that it may become too large even for modern and powerful computers, in particular for a very large number of undifferenced observations. However, no back substitutions or back smoothing is necessary in this case, which makes batch adjustment attractive in particular for DD approaches. Filter implementations for GNSS positioning are equivalent to sequential adjustments with steps coinciding with observation epochs. They are usually much more efficient and of smaller size than the batch adjustment implementations, at least as far as the position solutions with undifferenced observations are concerned. This is so, since parameters that appear only at a particular observation epoch, such as station clock and even ZTD parameters, can be preeliminated. However, filter (sequential adjustment) implementations require backward smoothing (back substitutions) for the parameters that are not retained from epoch to epoch (e.g., the station clock and ZTD parameters).

Furthermore, filter or sequential approaches can also model variations in the states of the parameters between observation epochs with appropriate stochastic processes that also update parameter variances from epoch to epoch. For example, the PPP observation model involves four types of parameters: station position (x_r, y_r, z_r), receiver clock (dt_r), troposphere zenith path delay (ZTD_w) and noninteger carrier-phase ambiguities (A_{IF}). The station position may be constant or change over time depending on the user dynamics. These dynamics could vary from tens of meters per second in the case of a land vehicle to a few kilometers per second for a low Earth orbiter (LEO). The receiver clock may drift and will have noise characteristics according to the quality of its oscillator, for example about 0.1 ns/s (equivalent to several cm/s) in the case of an internal quartz clock with frequency stability of about 10^{-10}. Comparatively, for a stationary receiver, the tropospheric ZTD will vary in time by a relatively small

amount, in the order of a few cm/h. Finally, the carrier-phase ambiguities will remain constant as long as the satellite is not being reoriented (e.g., during an eclipsing period, see the phase wind-up correction, Chap. 19 and Sect. 25.2.2) and the carrier phases are free of cycle slips, a condition that requires close monitoring. Note that only for DD data, i. e., two satellites observed from two stations, all clocks including the receiver-clock corrections are practically eliminated by the double differencing operation.

The system or process noise can be adjusted according to user dynamics, receiver-clock characteristics and atmospheric activity. In all instances the ambiguity process noise is set to zero, since the carrier-phase ambiguities remain constant over time. In static mode, the user position is also constant and consequently the coordinate process noise is also zero. In kinematic mode, it can be increased as a function of user dynamics, though usually the coordinate process noise values are set to a very large value to accommodate all possible user dynamics (including LEO satellites), effectively forcing independent position solutions for every epoch. The receiver-clock process noise can vary as a function of its frequency stability but is usually set to white noise with a large process noise variance to accommodate the unpredictable occurrence of clock resets. A random walk process noise of about 2–5 mm/$\sqrt{\text{h}}$ is usually assigned and used to drive the process noise variance of the ZTD. Note that for the most precise PPP applications, ZTD modeling typically also includes two additional stochastic (e.g., random walk) unknown parameters pertaining to the north-south and east-west ZTD gradients (Sect. 25.2.1).

Data Screening and Editing

When undifferenced code and phase observations are used, such as is the case for PPP, data testing and editing is quite essential (Chap. 24). For undifferenced, single-station observations this is a major challenge, in particular during periods of high ionospheric activity and/or station in the ionospherically disturbed subauroral or equatorial regions. This is because the difference between the phase observations on the two frequencies (e.g., GPS L1 and L2) along with widelane pseudorange/phase combinations (Chap. 20) are commonly used to check and edit cycle slips and outliers. Under quiet ionospheric conditions it is possible to detect and correct cycle slips even for data breaks exceeding 1 min, in particular when changes in ionospheric delays are taken into account [25.4]. When it is not possible to correct cycle slips a new initial ambiguity unknown has to be introduced. However, in the extreme cases of a highly active and scintillating ionosphere, this cycle slip editing approach would need data sampling higher than 1 Hz in order to safely edit or correct cycle slips or outliers. Due to memory constraints, data cannot always be sampled or processed at a rate of 1 Hz or higher. Within a geodetic receiver, however, it should be possible (at least in principle), to do efficient and reliable data cleaning and editing based on fitting the individual carriers phase measurements (e.g., φ_{L1} and φ_{L2}) or their difference ($\varphi_{\text{L1}} - \varphi_{\text{L2}}$), since data samplings much higher than 1 Hz are internally available. Most IGS stations have data sampling of only 30 s, which is why efficient statistical editing and error detection tests are critical, in particular for undifferenced, single station observation analyses.

On the other hand, the double-difference carrier-phase observations on the individual frequencies or even the DD ionosphere-free measurement combinations are much easier to edit or correct for cycle slips and outliers, consequently making statistical error detection and corrections less critical or even unnecessary. An attractive alternative for undifferenced observation network analyses is cycle slip detection and editing based on DD observations, which could also facilitate the resolution of the initial DD phase ambiguities. Resolved phase ambiguities are then reintroduced into the undifferenced analysis as the condition equations of the new undifferenced observations, formed from the reconstructed, unambiguous and edited DD observations, previously obtained.

25.2 Precise Positioning Correction Models

GNSS software must apply corrections to pseudorange observations in order to eliminate effects such as special and general relativity, Sagnac delay, satellite clock offsets, atmospheric delays, and so on (e.g., [25.7]; Chap. 19). Since these effects are quite large, exceeding several meters, they must be considered even for pseudorange positioning at the meter precision level. When attempting to combine satellite positions and clocks precise to a few cm with IF carrier-phase observations (with mm precision), or for the most precise differential phase processing mode, it is important to account for additional effects that are not normally considered for pseudorange positioning. An overview of the various model components and corrections in PPP applications is provided in Table 25.1.

Table 25.1 PPP a priori correction models. Magnitude and uncertainty values should be considered as approximate and may differ from case to case (after [25.27])

Model component		Magnitude	Uncertainty	Notes
Satellite	Center-of-mass position		2.5 cm (GPS)	Interpolated from precise orbit product in standard product 3 (format) (SP3) format with typical sampling of 15 min
	Antenna phase center offset	0.5–3 m	10 cm	Antenna offset vector in spacecraft system (IGS antenna exchange (ANTEX)) and GNSS specific attitude models [25.5, 6]
	Phase center variations	5–15 mm (GPS)	0.2–1 mm	IGS ANTEX model [25.5]
	Clock offset	< 1 ms	75 ps, 2 cm (GPS)	Interpolated from precise clock product with typical sampling of 30 s to 5 min
	Relativistic clock effects	10–20 m	–	Eccentricity-dependent effect [25.7, 8]
		2 cm	–	J_2-dependent contribution [25.8]; consistently neglected in current precise GNSS clock products and PPP models
	Differential code biases	up to 15 ns, 5 m	0.1–1 ns	Required biases depend on tracked signals and clock product [25.9, 10]
	Fractional phase biases	up to 0.5 cy	0.01 cy	For undifferenced ambiguity resolution [25.11]
Atmosphere	Troposphere (dry)	2.3 m	5 mm	Vertical delay [25.12], up to 10× larger for low elevations. Models: see, e.g., [25.13, Sect. 9.2], [25.14, 15]
	Troposphere (wet)	up to 0.3 m	up to 100%	Vertical delay [25.12]; estimated due to insufficient a priori models
	Ionosphere (1st-order)	up to 30 m	– / 1 m	Vertical delay, up to 3× larger for low elevations. Corrected through ionosphere-free combination (2-freq. PPP) or global ionosphere maps ([25.16]; 1-freq. PPP)
	Ionosphere (higher-order)	0–2 cm	1–2 mm	References [25.17] and [25.13, Sect. 9.4.1]
Site displacement				Corrections for expressing measured positions in a conventional terrestrial reference frame
	Plate motion	up to 0.1 m/y	0.3 mm/y	Reference [25.18]
	Solid Earth tide	up to 0.4 m	1 mm	References [25.19] and [25.13, Sect. 7.1.1]
	Ocean loading (tidal)	1–10 cm	1–2 mm	References [25.13, Sect. 7.1.2], [25.20, 21]
	Ocean loading (nontidal)	up to 15 mm	1 mm	Nonconventional correction; [25.22]
	Pole tide	25 mm	–	Reference [25.13, Sect. 7.1.4]
	Atmospheric loading (tidal)	up to 1.5 mm	–	Reference [25.13, Sect. 7.1.3]
	Atm. loading (nontidal)	up to 20 mm	15%	Nonconventional correction; [25.23]
Receiver	Phase center offset	5–15 cm	–	IGS ANTEX model (conventional values)
	Phase center variations	up to 3 cm	1–2 mm	IGS ANTEX model; [25.24]
Others	Phase wind-up	10 cm	see notes	Wavelength dependent; correction subject to knowledge of satellite/receiver antenna orientation; [25.25, 26]

For relative positioning at the cm-precision level and baselines of less than 100 km, all the correction terms discussed below can be safely neglected. The following sections describe additional correction terms often neglected in local relative positioning, that are, however, significant for PPP and all precise global analyses (DD or undifferenced approaches).

In the following discussion of PPP models, the correction terms have been grouped under four subsections covering propagation delays (Sect. 25.2.1), antenna effects (Sect. 25.2.2), site displacements effects (Sect. 25.2.3) and differential code biases (Sect. 25.2.4). Furthermore, compatibility considerations are addressed in Sect. 25.2.5.

A number of the corrections listed below require positions for the Moon and Sun (e.g., for tide and attitude computations). The respective information can be obtained from readily available planetary ephemerides files [25.28, 29], or more conveniently from simple analytical formulas [25.30–32], since a relative precision

of about 1/1000 is sufficient for corrections at the mm precision level.

25.2.1 Atmospheric Propagation Delays

Propagation of radio waves through the Earth's atmosphere introduces significant delays, which must be taken into account even for GNSS positioning at the meter precision level. For a comprehensive description of GNSS signal propagation see Chap. 6. Below are summarized the propagation delay models required for the highest precision PPP and GNSS global solutions as outlined in the current IERS2010 conventions [25.13].

Higher-Order Ionospheric Delay Corrections

The IF linear combination of dual-frequency observations used in (25.1) can be subjected to cm-level systematic errors caused by the neglected higher-order ionospheric delays. The higher-order ionospheric delays are negligible with respect to pseudorange noise of about 0.1–1.0 m but need to be considered for phase observations [25.33].

Following [25.13], the higher-order ionospheric delay errors of IF carrier-phase observations can be described as

$$d\varphi^{s}_{r,IF} = -\frac{s_2}{f_A f_B (f_A + f_B)} - \frac{s_3}{f_A^2 f_B^2}\,, \qquad (25.2)$$

where f_A and f_B denote the two signal frequencies (Hz) used in the IF combination.

The third-order term s_3 is negligible (at the sub-mm level) for GNSS frequencies. However, for a very high intensity ionosphere (such as during peaks of solar activity cycles) an s_3 ray-bending contribution, Δs_3, may become significant. For a given elevation E and slant total electron content (STEC), it can be approximated as

$$\Delta s_3 = b_1 \left(\frac{1}{\sqrt{1 - b_2 \cos^2(E)}} - 1 \right) \mathrm{STEC}^2 \qquad (25.3)$$

with $b_1 = 2.495 \cdot 10^8\,\mathrm{m\,MHz^4/TECU^2}$ and $b_2 = 0.8592$ [25.13, 34]. The slant total electron content can reach up to $\approx 300\,\mathrm{TECU}$ for a highly active ionosphere, where $1\,\mathrm{TECU} = 10^{16}\,\mathrm{electrons/m^2}$. Thus, $\Delta s_3 / f^4$ can reach up to 10 mm and should be considered here, along with the second-order term s_2, at least for the most precise GNSS solutions.

The s_2 coefficient of the second-order term can be approximated by

$$s_2 = 1.1284 \cdot 10^{12}\, B_p \cos(\Theta)\,\mathrm{STEC}\,, \qquad (25.4)$$

where $B_p \cos(\Theta)$ is the projection of the Earth's magnetic field intensity onto the satellite-station (i. e., satellite signal propagation) direction [25.13]. Equation (25.4) yields the value of s_2 in units of $\mathrm{m\,Hz^3}$ for STEC measured in electrons/$\mathrm{m^2}$ and B_p expressed in Tesla. The magnetic field strength required for the second-order correction can readily be obtained from models such as the international geomagnetic reference field (IGRF). Both the magnetic field B_p and the satellite station direction are taken at the piercing point on the adopted ionospheric shell (typically at a height of 450 km).

The STEC in (25.3) and (25.4) can be obtained from global ionosphere maps (GIMs) providing the vertical total electron content (VTEC) and a thin-shell mapping function (Chaps. 6 and 19). Such maps are, for example, generated by the IGS on a daily basis and distributed in the standardized ionosphere exchange format (IONEX); (Annex A). Alternatively, STEC can be evaluated from dual-frequency pseudorange-leveled carrier-phase observations after proper consideration of satellite- and receiver-specific differential code biases for the employed signals.

From (25.4) one can see that the second-order correction is highly geographically correlated, since it is a projection on the direction of the Earth's magnetic field, which is nearly the same within a wide area around the station. Furthermore, the direction of the Earth's magnetic field (mainly pointing north-south) is changing very slowly in time (nearly constant even over a decade). Therefore due to periodical changes of satellite geometry the second-order ionospheric refraction will cause small periodical errors, mainly in latitude. However, as seen from (25.4), the second-order ionospheric correction is also proportional to STEC, so it changes during the day (small at night, larger during the day). Finally, it can also be an order or even two orders of magnitude smaller (thus insignificant) during periods of low ionospheric activity than during periods of very active ionosphere.

In principle, the availability of three signal frequencies (such as GPS L1, L2, and L5) opens the possibility to eliminate the second-order ionospheric delay by an appropriate combination of the triple frequency observations [25.35]. However, in that case, because of additional biases connected with the third frequency observations, the compatibility with the standard dual-frequency solutions as well as a significant amplification of the observation noise [25.13] also need to be considered.

Tropospheric Delay Modeling

The tropospheric delay in (25.1) is commonly expressed as the product $T^s_r = M\,\mathrm{ZTD}$ of an elevation-dependent mapping function M and the zenith tro-

posphere delay ZTD. For all GNSS frequencies, the tropospheric delay T_r^s of (25.1) does not depend on frequency and the ZTD amounts to about 2.3 m at sea level. The ZTD can conveniently be divided into hydrostatic (dry) and wet components. The hydrostatic delay is caused mainly by the refractivity of the dry gases in the troposphere. The water vapor refractivity is responsible for most of the wet delay. Typically the hydrostatic delay component accounts for about 90% of the total delay (Chap. 6).

The hydrostatic delay (ZTD_h) can be accurately computed a priori from surface pressure p, station latitude φ and height h, using the formula of *Saastamoinen* [25.36] as given by [25.37]

$$ZTD_h = \frac{0.0022768\,\mathrm{m/hPa}\,p}{1-0.00266\cos(2\varphi)-2.8\cdot10^{-7}\,\mathrm{m^{-1}}\,h}\,. \tag{25.5}$$

For the smaller wet zenith delay (ZTD_w), there is no reliable model to obtain an a priori value. Because measuring the wet delay using water vapor radiometers is expensive and impractical for GNSS, it is normally estimated from the data. Standard GNSS navigation, utilizing pseudorange measurements or relative positioning over short baselines of a few tens of km, require only a simple mapping function M and a single a priori ZTD. In such cases, ZTD estimation is usually unnecessary or impossible. On the other hand, PPP and precise global solutions (Chap. 34) require that the ZTD mapping function M also be separated into a hydrostatic (dry) part (M_h) and a wet part (M_w). For the most precise GNSS applications, the ZTD north and east gradients (G_N, G_E) are also used, along with a gradient mapping function M_g. More specifically, the tropospheric delays of (25.1) are parameterized as

$$\begin{aligned} T_r^s &= M_h(E)\,ZTD_h + M_w(E)\,ZTD_w \\ &\quad + M_g(E)\,[G_N\cos(A) + G_E\sin(A)]\,, \end{aligned} \tag{25.6}$$

where A is the azimuth of the satellite direction and the gradient mapping function

$$M_g(E) = \frac{1}{(\sin(E)\,\tan(E)+0.0032)} \tag{25.7}$$

as suggested by [25.38] is typically used. The horizontal gradients (G_N, G_E) are needed to account for north-south atmospheric bulge and weather systems, since both can reach up to 1 mm [25.39].

Practically all the modern mapping functions use continued fractions

$$M(E,a,b,c) = \frac{1+\frac{a}{1+\left(\frac{b}{1+c}\right)}}{\sin E+\frac{a}{\sin E+\left(\frac{b}{\sin E+c}\right)}} \tag{25.8}$$

in terms of $\sin(E)$ as introduced by [25.40], where the coefficients a, b and c are small ($<<1$) constants. Different sets of coefficients (a_h, b_h, c_h) and (a_w, b_w, c_w) are required for the hydrostatic M_h and wet M_w mapping functions, respectively. Only the variation of the most significant coefficients a_h and a_w needs to be considered. The remaining and smaller coefficients (b and c) can use functional, mainly seasonal, representations.

For a self-contained PPP application with no external information input, the coefficients a_h and a_w can be obtained from global spherical harmonics expansions of mean geographical and seasonal variations, which is the case of the global mapping function (GMF) [25.14]. The more recent mapping function of the GPT2 (global pressure and temperature) model [25.41] uses global grids of mean values and mean seasonal or semiseasonal variations. The most precise PPP and GNSS applications use the Vienna mapping function 1 (VMF1) [25.42], which requires actual temporal and geographical variations of a_h and a_w, either site-specific or geographical grid files (with $2^\circ \times 2.5^\circ$ resolution). The VMF1 site-specific or grid files contain four sets of a_h and a_w coefficients per day (i. e., every 6 h), fitted to ray-tracing through the numerical weather model (NWM) of the European Centre for Medium-Range Weather Forecasts (ECMWF). The VMF1 site-specific or grid files, and alternatively those generated by the University of New Brunswick (UNB) and based on the US and Canadian NWMs [25.43], are readily available at [25.44] and [25.45], respectively.

Even though errors of the a priori ZTD_h (25.5) can be largely compensated by the ZTD_w estimation, for the most precise PPP and GNSS applications, ZTD_h needs to be known fairly accurately in order to properly separate the dry and wet ZTD mapping (25.6). According to [25.42], for a 5° elevation cutoff angle, the hydrostatic/wet mapping separation causes height errors of about one tenth of the ZTD_h error. This means that to reduce height errors below the mm level, the a priori ZTD_h has to be known at the cm-precision level, which in turn means that ZTD_h has to be based on measured pressure p, or more conveniently on p obtained from a NWM, for example the ones in the VMF1 grid files. The NWM grid files also contain ZTD_w, however, its uncertainty is at the 2 cm level, which is not sufficient for most PPP applications, and thus ZTD_w estimations are still required. Nevertheless, the NWM-based a priori ZTD_w can be used to significantly constrain ZTD_w

estimates, which may shorten the initial PPP solution convergence.

The VMF1 and UNB grid files require spatial and temporal interpolations of a_h, a_w and ZTD_h, ZTD_w for a specific station location and epoch [25.46]. Less precise, self-contained PPP solutions can use a constant ZTD_h, or one evaluated from (25.5) for a specific station location and epoch using the global pressure and temperature (GPT) model pressure [25.15]. Alternatively it can be obtained directly from the more recent GPT2 routine. Both GPT and GPT2 are based on global averages of NWM values and their seasonal variations. [25.47] investigated GMF and GPT performance and [25.43] compared GPT2-based PPP solutions with those using the VMF1 and UNB grid mapping functions and ZTD_h. Using a constant ZTD_h instead of a GPT- or GPT2-derived one may result in significant height errors due to hydrostatic/wet mapping separation errors. This is true in particular at high latitudes with large atmospheric pressure variations, where height errors can exceed 10 mm. It is interesting to note that a constant or GPT-derived ZTD_h and GMF, and to a smaller extend also the GPT2-derived values, tend to compensate the atmospheric loading effects on heights [25.46]. This explains why prior to atmospheric loading corrections, PPP solutions utilizing constant or GPT/GPT2 a priori ZTD_h, and/or GMF/GPT2 mapping functions may show slightly better height repeatability than the more accurate gridded VMF1 PPP solutions.

25.2.2 Antenna Effects

Phase Center Offsets and Variations

The ephemerides broadcast by today's GNSS satellites provide the position of the satellite antenna for direct use within the position computation. Here, no knowledge of the spacecraft orientation and antenna accommodation is required, but the achievable accuracy is limited in accord with the needs of pseudorange-based navigation. High-accuracy orbit products for PPP applications, in contrast, are referred to the spacecraft center of mass (CoM), which is the primary reference point for the orbit modeling. However, since GNSS measurements are effectively made between the phase centers of the transmitting and receiving antennas, it is necessary to account for the CoM offset of the satellite antenna and the orientation of the offset vector in space.

Representative values of the satellite antenna phase center offsets are summarized in Table 25.2 for the various constellations. The phase centers of all the GNSS satellites are offset by about one to a few meters in the body z-coordinate direction (towards the Earth) and some are also offset in the body x-coordinate direction, which is nominally in the plane containing the Sun, satellite and Earth.

In addition to the phase center offset in the spacecraft body frame, the orientation (attitude) of the spacecraft body relative to the terrestrial reference frame must be known to obtain the phase center position for given CoM coordinates of the GNSS satellite. Nominal attitude laws for the individual constellations and satellite types are discussed in [25.6] and Chap. 3. They allow computation of the satellite orientation for given orbital position and Sun direction and offer a good approximation of the true attitude except for short periods of noon and midnight turns during the eclipse season.

Since the assumption of a common phase center for all signals and line-of-sight directions is only approximately true for real antennas, complementary phase center variations (PCVs) need to be considered for high-precision carrier-phase modeling (Chaps. 17 and 19). Since November 5, 2006 (GPS Week 1400) the IGS has adopted calibration tables of absolute antenna PCV for both satellite and receiver antennas [25.5], which are readily available from the IGS [25.48] and updated as needed. The absolute PCV files (e.g., *igs08.atx* for consistent use with the IGS08/ITRF08 reference frame) contain PCV calibrations for all GNSS satellites and for practically all the receiver antenna models used by IGS. The receiver antenna PCV calibrations are usually based on antenna robot calibrations [25.24, 49] and include the measured phase center offsets (PCOs) together with elevation and azimuth dependent PCVs. The satellite portions of the absolute PCV file are based on solutions of several IGS analysis centers (ACs), which are consistent with the receiver antennas absolute PCVs and the IGS realization of the international reference frame.

It is advisable to use the absolute PCV convention in PPP solutions, for consistency with the orbits/clock computation process, but only when a receiver-absolute antenna PCV is available. If only a relative or no PCV calibration is available for the receiver antenna, then the nominal satellite antenna offsets and no satellite PCV should be used. PPP using absolute antenna PCV for satellite antennas with no or a relative receiver PCV may result in large (decimeter) solution errors and inconsistencies. Similarly, when orbits/clocks referred to satellite antenna phase center are generated from a network of ground stations (e.g., a commercial one) employing the same antenna types with no PCV, then PPP users with compatible antenna should not use any PCV either. However, when a user employs a different antenna than the one used to generate the orbits/clocks, the difference between the PCVs of the two antennas need to be accounted for.

Table 25.2 Antenna phase center offset from the center of mass for different types of GNSS satellites (after [25.6]). The offsets refer to IGS-specific spacecraft body axes and serve for illustration only. Satellite- and frequency-specific values used in the generation of IGS precise orbit and clock products are provided as part of the IGS ANTEX model (after [25.5])

Constellation	Type	*x* (m)	*y* (m)	*z* (m)
GPS	II/IIA	+0.28	0.00	+2.56
	IIR-A	0.00	0.00	+1.31
	IIR-B/M	0.00	0.00	+0.85
	IIF	+0.39	0.00	+1.60
GLONASS	M	–0.55	0.00	+2.30
	K1	0.00	0.00	+1.76
Galileo	In-orbit validation (IOV)	–0.20	0.00	+0.60
	Full operational capability (FOC)	+0.15	0.00	+1.00
BeiDou-2		+0.60	0.00	+1.10
Quasi-Zenith Satellite System (QZSS)	QZS-1	0.00	0.00	+3.20
Indian Regional Navigation Satellite System (IRNSS/NavIC)		+0.01	0.00	+1.28

Some modern receivers allow input of a receiver antenna PCV and output PCV corrected data, in such a case only the satellite antenna PCV should be considered when orbits/clocks refer to satellite centers of mass. When using the receiver independent exchange format (RINEX [25.50, Annex A]) for GNSS observations, data from receivers applying PCV corrections will report *NULLANTENNA* in the file header.

Phase Wind-Up

GNSS satellites employ right-hand circularly polarized (RHCP) electromagnetic waves for signal transmission, which means that the electric and magnetic field vectors perform a right-hand rotation about the propagation direction (Chap. 4). Other than linear polarization, the use of RHCP signals avoids restrictions on the relative orientation of the receive and transmit antenna and helps to mitigate multipath effects from reflected signals [25.51]. As a side effect, the measured carrier phase does not only change with the distance of the transmitter and receiver but also with the orientation of either of the two antennas relative to the line of sight. This is known as *phase wind-up* [25.25] and will, for example, result in a phase change by one cycle for a full rotation of the receive or transmit antenna about the boresight direction. It should be noted that only the carrier phase measurements are sensitive to wind-up effects, whereas the pseudorange observations remain unaffected (Chap. 19).

Phase wind-up effects have commonly been neglected in differential positioning applications since the effects are highly correlated for stationary receivers with a separation of less than a few hundred kilometers. For mobile receivers the phase wind-up caused by a rotation of the receiver antenna about a fixed axis is identical for all received satellites. Thus, it can partly be absorbed in the clock solution, but will give rise to a code-carrier inconsistency when processing both pseudorange and phase observations. Consideration of the user antenna orientation and the resulting phase wind-up is therefore essential for precise positioning on mobile platforms with continued attitude changes [25.26]. In particular, phase wind-up effects must be properly modeled for a toggling antenna [25.52], where the rotation vector varies over time.

Even for a presumably stationary position and alignment of the receiver antenna, phase wind-up effects arise from the slowly changing relative orientation of the satellite antenna, line of sight, and receiver antenna. Following [25.25] the resulting carrier phase change may differ by up to 4 cm for two stations separated by 4000 km.

GNSS satellites need to continuously change their orientation about the Earth-pointing antenna axis to orient their solar panels towards the Sun. Irrespective of the user antenna dynamics, these satellite attitude changes will results in a measurable phase wind-up effect. They are most pronounced during noon and midnight turns in the eclipse season, where the satellites may rotate by up to 180° (corresponding to a phase wind-up effect of half a wavelength) in 15–30 min. If ignored, these are fully absorbed into the estimated satellite clocks and thus are completely eliminated by double differencing. They become important, however, for undifferenced PPP applications and need to be consistently handled in the generation of orbit/clock products and the user positioning software. Within the IGS, phase wind-up effects are considered by all analysis centers and their respective products. Neglecting them and fixing IGS orbits/clocks in a PPP process may result in position and clock errors at the dm level.

Details of the phase wind-up modeling and the applicable satellite attitude models are provided in Chap. 19. Aside from nominal attitude laws, dedicated models have been developed for describing the noon or midnight turns of various types of satellites during the eclipse season [25.53–55]. Unless these models can be consistently applied by the user, the respective satellites and time intervals should be discarded in the PPP processing.

As an alternative to rigorous phase wind-up modeling, the use of a *decoupled clock model* has been suggested in [25.56]. Here unmodeled wind-up effects that otherwise result in a code-carrier inconsistency are absorbed in distinct clock offset parameters for the pseudorange and carrier-phase observation model. This approach can be applied if external attitude information for the receiver antenna is not available and the antenna is primarily rotating about a constant axis.

25.2.3 Site Displacement Effects

By its very nature, precise point positioning delivers coordinates in a global terrestrial reference frame such as the international terrestrial reference frame (ITRF) or the IGS-specific IGSyy frame. The realization of such a frame is complicated by the fact that the Earth and its crust are not perfectly solid. The various forces acting on the Earth (e.g., lunar and solar gravity, but also loading due to ice, oceans and even the atmosphere) result in periodic deformations and thus periodic motion of individual stations. These are mostly highly correlated over large areas and can therefore be neglected in relative positioning over up to a few hundred km. However, the periodic motions have been removed through relevant models in the realization of the ITRF and its reference station coordinates. In accord with current IERS conventions [25.13], the same models of the periodic site displacements must be accounted in all PPP applications to obtain ITRF-compatible site positions.

Dominant effects such as solid Earth and pole tides or ocean loading cause site displacements at the few cm to dm level and are discussed below in further detail. Effects with a magnitude of less than 1 cm, such as surface loading from atmospheric pressure, ground water and/or snow buildup, are neglected and not considered in the following. These small effects can be applied a posteriori or even monitored with PPP solutions (e.g., local ground water/snow buildup variations). For these reasons, no IGS solutions currently include the above-mentioned environmental loading effects. Furthermore, diurnal and semidiurnal atmospheric tides S_1 and S_2, included in the IERS2010 conventions and applied by some IGS analysis centers have also been neglected here. The vertical amplitudes of S_1 and S_2 can reach up to about 2 mm, mainly in the equatorial regions, and they will largely average out over the standard 24 h solution periods used by IGS. The horizontal S_1/S_2 effects are about one order of magnitude smaller, so for all kinematic and most static PPP solutions, the horizontal and even vertical atmospheric tides can be neglected.

Solid Earth Tides

Similar to ocean tides, the gravitational attraction of the Sun and Moon causes a subtle deformation of the (presumably solid) Earth and its crust. It results in horizontal and vertical displacements that can be modeled by a spherical harmonics expansion and associated physical parameters (known as Love and Shida numbers), which describe the susceptibility of the Earth's body to the tide-generating potential. At an accuracy level of about 5 mm, it is sufficient to only consider the dominant, second-degree tides of the Sun and Moon along with a supplementary height correction term [25.57]. Within this approximation, the site displacement of a station at position $\boldsymbol{r}$ can conveniently be described by the geocentric unit vectors $\boldsymbol{e}_\odot = \boldsymbol{r}_\odot/r_\odot$, $\boldsymbol{e}_\leftmoon = \boldsymbol{r}_\leftmoon/r_\leftmoon$, and $\boldsymbol{e} = \boldsymbol{r}/r$ in Sun, Moon, and station direction

$$\begin{aligned}\Delta\boldsymbol{r} = \sum_{j=\odot,\leftmoon} \frac{GM_j}{GM_\oplus}\frac{r^4}{R_j^3}\Bigg\{&\left[3\mathrm{l}_2\left(\boldsymbol{e}_j\cdot\boldsymbol{e}\right)\right]\boldsymbol{e}_j \\ &+\left[3\left(\frac{\mathrm{h}_2}{2}-\mathrm{l}_2\right)\left(\boldsymbol{e}_j\cdot\boldsymbol{e}\right)^2-\frac{\mathrm{h}_2}{2}\right]\boldsymbol{e}\Bigg\} \\ &+\left[-0.025\,\mathrm{m}\sin\varphi\cos\varphi\sin\left(\theta_\mathrm{g}+\lambda\right)\right]\boldsymbol{e}\,.\end{aligned} \tag{25.9}$$

Here, $GM_\oplus$, $GM_\odot$, $GM_\leftmoon$ are the gravitational coefficients of the Earth, Sun, and Moon, while $\mathrm{l}_2 = 0.6090$ and $\mathrm{h}_2 = 0.850$ are the nominal second-degree Love and Shida numbers. The height correction term in (25.9) is described in terms of the station latitude φ and longitude λ as well as the Greenwich mean sidereal time θ_g.

For an accuracy of 1 mm or better further harmonics and the dependence of Love and Shida numbers on the station location and the frequency of each tidal constituent need to be considered [25.13, 58]. To facilitate a consistent application of the respective corrections, suitable computer implementations are made available along with the IERS conventions [25.13].

Overall, the solid Earth tides induce vertical station displacements of about 0.3 m and horizontal displacements of about 5 cm. Aside from periodic contributions with a dominating half-daily and daily periodicity, the tidal correction (25.9) also comprises a permanent displacement at the 1 dm level. Even though the periodic terms are largely averaged out in the processing of daily

arcs for static sites, the same does not apply for the permanent tidal displacement. Irrespective of the data arc and type of site, consideration of the full solid Earth tide correction is therefore essential in all PPP applications to comply with the *tide-free* ITRF realization.

Rotational Deformation due to Polar Motion (Pole Tide)

Aside from luni-solar tidal forces, small periodic changes in the deformation of the Earth are also caused by polar motion, that is, by changes in the location of the Earth's rotation axis relative to its crust. Following [25.13], the associated site displacements in east, north and up direction are given by

$$\begin{aligned}\Delta r_{\mathrm{E}} &= +9\,\mathrm{mm}\cos\theta\,[m_1\sin\lambda - m_2\cos\lambda]\,,\\ \Delta r_{\mathrm{N}} &= +9\,\mathrm{mm}\cos 2\theta\,[m_1\cos\lambda + m_2\sin\lambda]\,,\\ \Delta r_{\mathrm{U}} &= -33\,\mathrm{mm}\sin 2\theta\,[m_1\cos\lambda + m_2\sin\lambda]\,,\end{aligned} \tag{25.10}$$

for a station at longitude λ and colatitude $\theta = \pi/2 - \varphi$. Here $m_1 = (x_{\mathrm{p}} - \bar{x}_{\mathrm{p}})$ and $m_2 = -(y_{\mathrm{p}} - \bar{y}_{\mathrm{p}})$ (expressed in [″]) are the coordinates of the Earth's rotation pole in the terrestrial reference frame, which are obtained as the difference of the polar motion variables $(x_{\mathrm{p}}, y_{\mathrm{p}})$ and the IERS model [25.13, Table 7.7] of the mean pole $(\bar{x}_{\mathrm{p}}, -\bar{y}_{\mathrm{p}})$.

Polar motion is not predictable, but exhibits dominating variations with periodicities of about 430 d (Chandler period) and 365 d (annual period). At amplitudes of up to 0.8″, the site displacements due to the pole tide may amount to roughly 25 mm in the vertical direction and about one quarter of this value in horizontal direction.

Polar motion centrifugal effects on the oceans cause an analogous ocean pole tide loading, also considered in the IERS2010 conventions. It also has seasonal and Chandler period variation, but it is rather small, nearly an order magnitude smaller than the above polar tides, so it can be safely neglected in most PPP applications.

Ocean Loading

Ocean tides result in a varying load of sea water and associated deformations of the Earth's crust. The induced site displacement is most pronounced in the vertical direction and typically at the cm level. However, in coastal regions, ocean loading can result in coordinate changes of up to 10 cm [25.20]. The response of the Earth's surface to the load changes depends largely on the topography and is typically not aligned with the body tides [25.59]. As with solid Earth tides, ocean loading effects show predominant semidiurnal and diurnal periodicities but, by convention, do not exhibit a permanent part.

Given these characteristics, ocean loading may be neglected for static positioning over daily periods, stations far off (typically > 1000 km) the coast or moderate accuracy requirements. However, it clearly needs to be considered for kinematic positioning, cm-level accuracy and coastal regions. As pointed out by [25.60], unmodeled ocean loading effects may also contaminate tropospheric ZTD or station clock estimates, which are highly correlated with the vertical position.

In its most basic form, coordinate shifts Δc due to ocean loadings are described as a harmonic series

$$\Delta c = \sum_{j=1}^{11} A_{\mathrm{c}j}\cos(\chi_j(t) - \phi_{\mathrm{c}j}) \tag{25.11}$$

for each of three coordinate axes [25.13]. The individual terms considered in these series correspond to one of 11 semidiurnal (M_2, S_2, N_2, K_2), diurnal (K_1, O_1, P_1, Q_1), and long-period (M_{f}, M_{m} and S_{sa}) tide waves. The time-dependent angles χ_j are linear combinations of fundamental astronomical arguments such as the mean longitudes of the Sun and Moon and can consistently be computed using reference software implementations provided by the IERS [25.13]. The amplitudes $A_{\mathrm{c}j}$ and phases $\phi_{\mathrm{c}j}$, on the other hand, are station-specific quantities computed from global ocean tide models [25.61]. For a specific site and ocean tide model, these values can be conveniently obtained from an ocean loading provider service [25.62].

The ocean loading also induces periodic tidal variations of the Earth's center of mass (CoM) relative to a crust-fixed system aligned with the mean center of the Earth. These CoM offsets may be evaluated using an expression similar to (25.11) [25.13], but are not normally required for PPP users, since GNSS orbits products as provided by the IGS are, by convention, referred to a crust-fixed frame such as the ITRF.

25.2.4 Differential Code Biases

The observation model discussed in Sect. 25.1.1 is based on the simplifying assumption that all measurements are free of any biases. While this assumption is not necessarily true, it offers a proper model in practice, provided that GNSS clock products are generated with the same type of observations as used for the precise point positioning. For GPS, published clock offsets (in both the broadcast ephemerides and the precise products) are conventionally referred to an ionosphere-free combination of P(Y)-code observations on the L1 and L2 frequencies. Similarly, GLONASS precise clock products are based on L1/L2 P-code observations. When using the same signals for PPP, no further code

biases need to be considered and the observation model (25.1) can be used as is.

The situation is different, though, when working with other types of dual-frequency signals (e.g., the civil L1 C/A or L2C codes). In this case satellite-specific differential code biases (DCB) have to be applied to account for group delay differences between the signals tracked by the receiver and those of the clock reference signal [25.63]. A common application case is dual-frequency GPS PPP using commercial receivers that do not provide distinct P(Y)-code observations on L1, but deliver only C/A-code pseudoranges. Here, a supplementary bias

$$\frac{f_{\mathrm{L1}}^2}{f_{\mathrm{L1}}^2 - f_{\mathrm{L2}}^2} \mathrm{DCB}^{\mathrm{s}}_{\mathrm{C1C\text{-}C1W}} \tag{25.12}$$

needs to be added in the observation model (25.1) for the ionopshere-free pseudorange to translate the satellite clock offset and make it compatible with the employed observations. In the above equation

$$\mathrm{DCB}^{\mathrm{s}}_{\mathrm{C1C\text{-}C1W}} = d^{\mathrm{s}}_{\mathrm{C1C}} - d^{\mathrm{s}}_{\mathrm{C1W}} \tag{25.13}$$

denotes the differential code bias of L1 C/A and L1 P(Y) pseudorange observations (indicated here by the corresponding RINEX observation codes C1C and C1W [25.50]). It may be noted that no receiver biases need to be considered in single-constellation processing, since those can readily be absorbed in the receiver-clock bias estimate. As an exception, such biases need to be calibrated and taken into account in PPP-based time transfer as further discussed in Chap. 41.

In multi-GNSS processing, satellite-specific DCBs need to be individually considered for a constellation whenever the tracked signals are different from the clock reference signals. In addition, an intersystem bias needs to be adjusted to compensate for time system differences between constellations and receiver-specific differential code biases (Chap. 21 and [25.63]).

DCBs of GPS and GLONASS satellites are routinely determined by various IGS analysis centers as part of their ionospheric analysis [25.16] for the legacy signals on L1 and L2. DCBs for the multitude of new signals and constellations are, furthermore, determined by the IGS from observed code differences and global ionosphere maps [25.10]. Use of these biases assists a more rigorous modeling of pseudorange observations. Even though PPP performance is generally driven by the high precision of carrier-phase observations, and partly *tolerant* to pseudorange errors, the proper consideration of DCBs is known to improve the convergence time in filter-based implementations and to enable a faster and more reliable ambiguity fixing.

25.2.5 Compatibility and Conventions

Precise point positioning fixes (or tightly constrains) external data such as the GNSS orbits and clock offset values. To ensure the desired cm- or mm-level accuracy, the PPP models and algorithms must be highly consistent with those used in the generation of the auxiliary products. Since PPP is in fact equivalent to a station position solution within a global network solution (but conveniently condensed within the precise orbit/clock products), it must adhere to the same conventions used in extracting orbit and clock data from the network. Among others, this may affect the choice of reference frames, Earth orientation parameters, antenna offset and phase pattern or the application of specific model corrections.

Within the IGS, which serves as a primary source of freely available high-accuracy GNSS data and products for scientific users, orbit and clock products are generated by various analysis centers (ACs). These adhere to common standards such as the IERS conventions (currently [25.13]), reference frames (currently ITRF2008/IGS08), and antenna phase center calibration models (currently *igs08.atx*, [25.48]). Clock products for GPS and GLONASS are based on ionosphere-free combinations of P(Y)-or P-code observations on the L1 and L2 frequencies and have been corrected for the eccentricity-dependent periodic relativistic clock variation. For other constellations, initial products provided within the IGS multi-GNSS experiment (MGEX) [25.64] are based on ionosphere-free E1/E5b (Galileo) or B1/B2 (BeiDou) combinations, but no formal standard has been established yet.

An overview of past and current conventions for the use of IGS products in PPP applications is provided in [25.65]. For specific and detailed information in a standardized format on each IGS AC global solution strategy, modeling and departures from the conventions, refer to the IGS central bureau archives [25.66].

25.3 Specific Processing Aspects

The concept of precise point positioning was originally developed for use with dual-frequency GPS observations, but is highly generic and can be applied to a variety of signals and constellations. Even though the basic modeling techniques discussed before are valid for all forms of PPP, some variants deserve specific consideration. Within the present section, single-frequency PPP is first discussed (Sect. 25.3.1), which is of particular interest for use with low-cost GNSS receivers. The use of GLONASS observations brings the added complexity of channel-dependent biases and is addressed in Sect. 25.3.2, while the use of new signals and other constellations is discussed in Sect. 25.3.3. Finally, PPP ambiguity fixing concepts are presented in Sect. 25.3.4, which offer a substantial increase in accuracy as well as a notably improved convergence time in sequential processing.

25.3.1 Single-Frequency Positioning

Traditional single-frequency point positioning (PP) utilizes pseudoranges only. If carrier-phase observations are available, they are commonly used for smoothing of pseudoranges, often internally within the receiver, in order to reduce pseudorange measurement noise [25.67]. The phase-smoothed pseudoranges are then used, along with ionospheric models (e.g., the broadcast Klobuchar model or global ionosphere maps [25.16]) to account for significant ionospheric delays [25.68–70]. Single frequency PP can use either the broadcast or more precise post-mission orbit/clock solutions. The broadcast and precise orbit/clocks are typically determined from dual-frequency data, so the satellite clocks reflect the corresponding differential code biases (e.g., the $\mathrm{DCB}_{\mathrm{C1W-C2W}}$ of GPS P(Y)-code pseudoranges on the L1 and L2 frequencies), which change from satellite to satellite and can reach several meters. Since single-frequency GPS receivers most commonly track the civil C/A-code signal rather than the encrypted P(Y)-code, an additional $\mathrm{DCB}_{\mathrm{C1C-C1W}}$ must be considered as well. For real-time use, equivalent timing group delay (TGD) and intersignal correction (ISC) parameters are transmitted as part of the modernized GPS navigation message [25.63, 71]. Neglecting these biases can cause positioning errors larger than when ionospheric delays are neglected [25.72]. The traditional, single-frequency PP is typically used for m-level navigation solutions only with four unknowns (three position coordinates and one clock). In such PP solutions, except for antenna offsets and a nominal tropospheric delay, practically all the effects discussed in Sect. 25.2 can be safely neglected.

A more precise alternative to single-frequency pseudorange PP is single-frequency PPP utilizing the code-plus-carrier (CPC) or GRAPHIC (group and phase ionospheric calibration [25.73]) combination $o_{\mathrm{GPH}} = (p+\varphi)/2$ of pseudorange and phase observations on the same frequency. It is ionosphere-free (to first order), since the ionospheric code and phase delays are the same, but of opposite signs. Namely, the carrier phases are advanced (shortened) and pseudoranges are delayed (lengthened) by the ionosphere (Chap. 19). Consequently, the new observable has a significantly lower observation noise (by a factor of two) than the original pseudorange and requires no external ionospheric information or corrections. However, due to the use of carrier phases, is subject to an ambiguity. This necessitates the use of pseudoranges and solving for ambiguities, much like in case of the standard dual-frequency PPP. This also results in a fairly long solution convergence (15 min or longer).

Many of the models and effects discussed above (Sect. 25.2) also need to be considered here, since the GRAPHIC-based PPP precision is at a few dm (Fig. 25.1). This applies specifically to tidal site displacement effects but also to carrier-phase wind-up when working with rotating and tumbling platforms [25.26]. As with the dual-frequency carrier-phase combination, the code-plus-carrier combination is not rigorously ionosphere-free but likewise includes some second- (and third-) order contributions. These are typically buried in the observation noise and multipath but may be taken into account in case of high ionospheric activity and when working with high-performance ranging signals.

The observation model for the single-frequency GRAPHIC combination is given by

$$\frac{1}{2}\left(p_{\mathrm{r}}^{\mathrm{s}}+\varphi_{\mathrm{r}}^{\mathrm{s}}\right)=\rho_{\mathrm{r}}^{\mathrm{s}}+c\left(dt_{\mathrm{r}}-dt^{\mathrm{s}}\right)+T_{\mathrm{r}}^{\mathrm{s}} +\lambda A_{\mathrm{GPH}}+\frac{1}{2}\lambda\omega+e_{\mathrm{GPH}}\,, \qquad (25.14)$$

where ω denotes the phase wind-up effect and $A_{\mathrm{GPH}} \approx -N/2$ is the (float valued) GRAPHIC ambiguity. It lumps minus one half of the carrier phase ambiguity as well as differential code biases between the employed single-frequency pseudorange observation and the (dual-frequency) code observations used for the satellite clock product. These DCBs need also be considered when combining the GRAPHIC observations with (single-frequency) pseudoranges to enable estimation of both the receiver clock offset and the GRAPHIC ambiguities. Depending on the accuracy

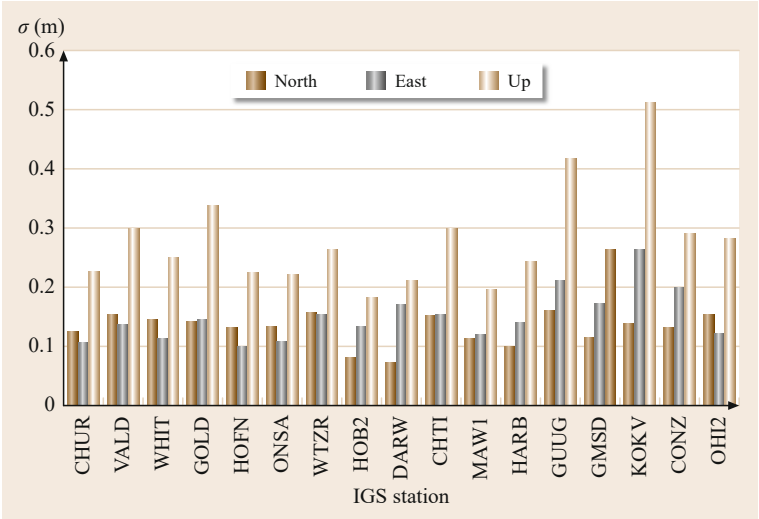

Fig. 25.1 Repeatability of single-frequency kinematic PPP solutions at 17 globally distributed IGS stations obtained with IGS final orbits/clocks over a one-year period (Jan. 1, 2012–Feb. 9, 2013). The employed GRAPHIC observations are based on GPS L1 P(Y)-code and phase measurements. Individual *bars* for each station indicate the precision of the north, east, and up (height) components

requirements, tropospheric delays in (25.14) may be considered through models or estimated as in the case of dual-frequency PPP [25.74].

Except for very short data arcs that do not enable proper estimation of the ambiguities, the GRAPHIC-based PPP solution usually offers better positioning results than single-frequency pseudorange processing with a priori corrections from global ionosphere maps [25.75]. As discussed in [25.76], sub-decimeter accuracy (3-D RMS) can be achieved for least-squares solutions using batches of at least 6 h duration solutions. The ionosphere-free code-plus-carrier combination appears particularly attractive for use with advanced ranging signals such as the Galileo E5 alternative BOC (AltBOC) signal. Even though the GRAPHIC processing is not fully competitive to dual-frequency PPP, a three- to four-fold performance increase has been demonstrated in [25.77] when using AltBOC in comparison with legacy GPS L1 C/A observations. Due to the very low noise and high multipath resistance of this signal, 3-D RMS positioning accuracies of 20 cm down to 3 cm can be achieved with data arcs of 1–24 h.

As an alternative to the ionosphere-free code-plus-carrier processing, the direct processing of pseudorange and carrier-phase estimation has been proposed in [25.78] along with the estimation of the vertical total electron content (VTEC) and a common mapping function. Due to different pierce points a common VTEC for all observations is not appropriate though, and horizontal ionospheric gradients have to be estimated as well in this approach.

Irrespective of the specific formulation of the single-frequency PPP algorithms, a reliable detection and handling of cycle slips is vital for achieving a high overall performance. Since GRAPHIC observations may exhibit a noise level above the (half) carrier-phase wavelength, single-cycle slips may be hard to identify on this combination alone. Cycle-slip detection (and repair) techniques based on time-differenced carrier-phase observations and a geometry-based approach that overcome these difficulties are discussed in [25.79].

25.3.2 GLONASS PPP Considerations

Next to GPS, the Russian GLONASS was the second global navigation satellites system considered for precise point positioning [25.80, 81]. A joint use of both constellations promises notably improved convergence times and robustness, even if the accuracy of the estimated positions remains similar to that of GPS-only solutions [25.82–84].

However, the processing of GLONASS observations is complicated by the frequency division multiple access (FDMA) modulation scheme (Chap. 8), which makes use of slightly different signal frequencies on about 15 distinct channels. The individual channels are separated by 562.5 kHz and 437.5 kHz for L1 and L2, respectively (Chap. 8) and may result in interfrequency-channel biases (IFCB) for both code and phase observations. These biases affect the generation of precise orbit and clock products as well as the use of GLONASS observations for precise point positioning.

Depending on the receiver design, notable group delay variations across the different frequency channels may be encountered. Receiver-specific pseudorange IFCBs can exceed ±10 m and usually tend to have a linear behavior with rates up to about ±2 ns per channel index. The biases tend to be similar for the same receiver type, though antenna model and receiver model, or even a different receiver firmware version may

cause atypical behavior (Fig. 25.2). When GLONASS pseudoranges are weighted with sufficiently large uncertainty (e.g., 10 m), the pseudorange IFCBs have no significant effect (i. e., sub-mm) on PPP position and ZTD solutions but affect the receiver clock solutions. So in principle, pseudorange IFCBs need not cause significant problems in PPP solutions, unless ambiguity fixing is attempted (Sect. 25.3.4).

Aside from pseudorange IFCBs, GLONASS observations are also affected by carrier-phase IFCBs. These may differ by up to 5 cm per channel index between different receiver brands [25.85] and notably affect the ambiguity resolution in both differential and undifferenced (PPP) processing schemes. However, those small frequency-dependent phase biases are largely deterministic and can be attributed to group delays and digital delays in the signal processing that differ between receivers. They can essentially be eliminated when pseudorange and phase observations are made at the same sampling epoch [25.86].

To cope with these issues and to facilitate a consistent processing of GNSS observations from different receivers, current versions of the RINEX standard [25.50] specify a mandatory phase alignment of the GNSS measurements prior to generating the RINEX observations file. Consequently, for properly generated RINEX GLONASS data there should not be any phase IFCBs.

Provided that all the GNSS processes are using consistent and sufficiently precise observations and modeling, apart from distinct clocks solutions, each GNSS-specific PPP solution should then yield statistically equivalent position and ZTD solutions. This is confirmed, for example, in a performance assessment of [25.84] and independently illustrated in Fig. 25.3. The figure provides a comparison of GPS and GLONASS PPP solutions for selected IGS reference stations over a 13-month period. Differences between the GPS-only solution and the GLONASS-only solutions as well as deviations from the known IGS08 positions of the stations are generally at the few-mm level and most mean offsets are statistically insignificant when the real accuracy of PPP is considered (Sect. 25.5).

It is interesting, though, to note that GNSS-specific PPP solutions are fairly independent despite the fact that the measurements are observed by the same instrumentation (receiver/antenna). This is due to different observation sets, different satellite modeling and even local environmental effects (such as multipath and subdaily station movements), which may be somewhat different due to different constellation-specific satellite geometry, signal strength and/or frequencies. For example, GLONASS-GPS daily static PPP position solution differences at coastal stations may exhibit significant fortnight periodical signals (exceeding the repeatability sigmas) when ocean loading is neglected or wrongly applied. Satellite geometry and its repeatability likely cause this, since they are different for GPS and GLONASS. In this regard, different GNSSs may facilitate an important verification of individual PPP solutions.

25.3.3 New Signals and Constellations

The ongoing modernization of the GPS and GLONASS constellations as well as the buildup of new global and regional navigation satellite systems (BeiDou, Galileo, QZSS, IRNSS/NavIC) offers new prospects for improved PPP performance but poses also a variety of challenges to their users.

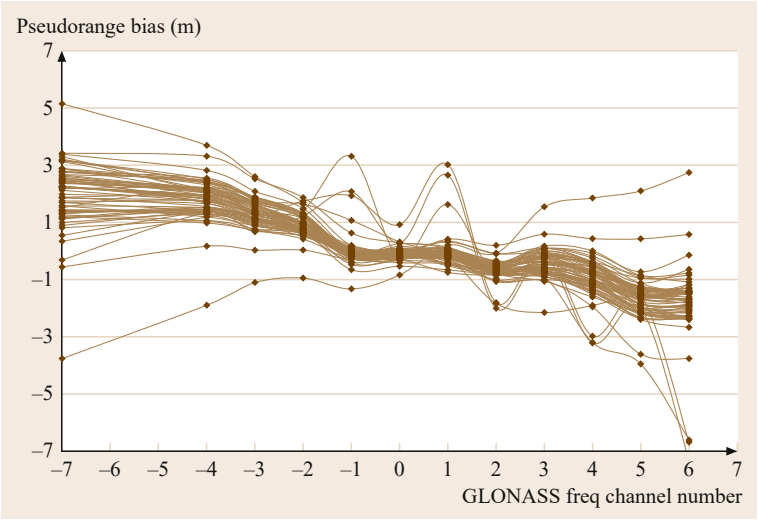

Fig. 25.2 GLONASS interchannel pseudorange biases for a group of Leica receivers as determined on March 1, 2013. Most atypical biases seen here are due to different antennae or old receiver firmware

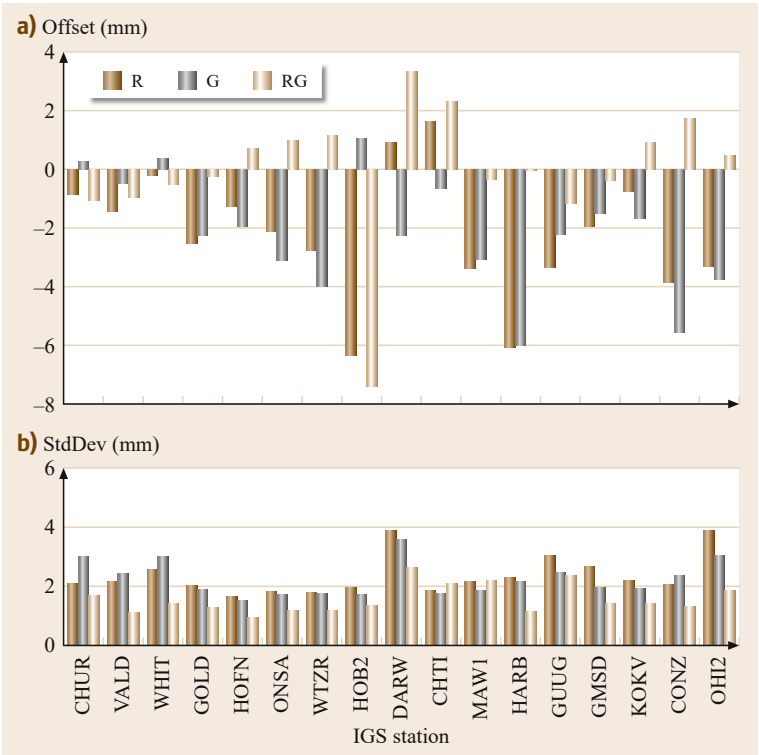

Fig. 25.3a,b Performance of static daily PPP solutions using GLONASS and GPS observations for 17 globally distributed IGS stations between 1 Jan. 2012 and 9 Feb. 2013 using European Space Agency (ESA) final GPS/GLONASS orbit/clock products. The graphs show the mean offset **(a)** and standard deviation **(b)** of the north position component for GLONASS-only processing (R) and GPS-only processing (G) relative to the IGS08 reference position as well as the difference of the two solutions (RG). Similar but slightly larger values apply for the scatter of the east and height components but no significant biases are obtained (not shown)

As discussed before, PPP depends critically on the consistency of auxiliary products (specifically the GNSS orbits and clocks) and the user processing. While relevant standards and conventions have evolved for GPS and GLONASS legacy signals over many years, they still need to be established for new signals and constellations. Along with that comes a need to thoroughly characterize the space segment (satellites, attitude laws, transmit antennas, biases) and the user segment (receivers, antennas, biases) in order to fully exploit the performance offered by the multitude of new signals in space.

While consistency of processing schemes, algorithms and even equipment can readily be ensured by commercial PPP service providers taking care of both the orbit/clock product generation and their usage, a larger effort is required for public services such as the IGS, which need to deal with a variety of different end-user equipment and possible processing tools. Such work has been initiated by the IGS within its Multi-GNSS experiment (MGEX; [25.64]) and resulted in the evolution of standards for the real-time and offline exchange of observation and navigation data (RINEX, RTCM; Annex A), conventional attitude models for all GNSS satellites [25.6], multifrequency receiver antenna calibrations [25.87], differential code biases for open signals of the various constellations [25.10] as well as early orbit and clock products for Galileo [25.88], BeiDou [25.89], and QZSS [25.90] or several of these new constellations [25.91, 92]. Even though the precision and accuracy of multi-GNSS products and system characterizations still lags behind GPS and GLONASS, continued efforts are made to improve their performance and to make them fully competitive.

As a straightforward extension of the GPS-only or GPS-GLONASS PPP concept discussed before, ionosphere-free combinations of pseudorange and phase observations of dual-frequency signals may be processed for any individual constellation or any combination of two or more constellations. When combining signals from multiple constellations, an intersystem bias (assumed to be constant over the processing arc) needs to be estimated for all but one constellation to compensate for possible system time offsets and constellation-specific receiver biases ([25.63, 93–96] and Chap. 21). Furthermore, satellite-specific DCBs will need to be applied, if the employed signals differ from those used in the generation of the respective clock product. The choice of signals used for the individual constellations will depend on availability (all satellites in the constellation should transmit the selected signal to avoid the presence of additional biases), signal characteristics (C/N_0, multipath resistance, etc.), and the employed clock product. Obviously, the two frequencies should be

widely spaced to minimize the noise of the ionosphere-free combination (allowing, e.g., GPS L1/L2 or L1/L5, but ruling out GPS L2/L5 as a meaningful option).

Initial results of multi-GNSS PPP processing involving BeiDou and/or Galileo next to GPS and GLONASS have, for example, been reported in [25.92, 97–99]. They confirm the benefit of an increased number of signals in space for the robustness and convergence time of PPP solutions and demonstrate an improved accuracy when applying state-of-the art models. The combination of signals from multiple constellations is of particular interest in constrained environments, which inhibit the use of low-elevation signals. Here, the minimum number of satellites required for kinematic point positioning (four to seven depending on the number of constellations and constellation-specific intersystem biases) can be ensured for cutoff angles as high as 40° in the combined GPS, GLONASS, BeiDou and Galileo service area [25.100]. Even though other constellations than GPS and GLONASS do not yet offer a fully global availability, multi-GNSS PPP is an emerging trend that will help to further improve PPP performance but also enables a better understanding of possible systematic errors that may go undetected in single-system solutions.

Along with the integration of the new constellations into the traditional, dual-frequency PPP concept, efforts are made to allow a seamless use of signals on more than just two frequencies into the PPP processing. This is of interest, since civil (or at least publicly accessible) signals are made available on three or even more frequencies by various new or modernized navigation satellite systems (including, so far, GPS L1/L2/L5, Galileo E1/E5a/E5b/E6, QZSS L1/L2/L5/E6, and BeiDou B1/B2/B3). A possible approach consists of the joint processing of multiple ionosphere-free dual-frequency combinations (e.g., GPS L1/L2 as well as GPS L1/L5). However, special care needs to be taken in this case to account for the correlation introduced by the repeated use of the same measurements (here L1) in the combined observations [25.101].

For a unified treatment of multiple signals, an uncombined, or *raw*, processing approach is followed in [25.102–104], which uses uncombined code and phase measurements on each of the available frequencies and introduces ionospheric slant delays as additional (epoch-wise) estimation parameters. With an undifferenced formulation one has the advantages of being able to use the simplest observational variance matrix and having all the parameters remain available for a possible further model strengthening. This latter aspect allows one to take advantage for instance of the time stability of biases or next-generation satellite clocks. Parameters that are not considered of interest can then easily be eliminated through the reduction of the normal equations, instead of performing an a priori elimination at the observational level that usually comes at the expense of a more complicated structure of the observational variance matrix. So far, experience with the *raw* PPP approach is limited due to the small number of satellites transmitting triple-frequency signals as well as time-varying biases between the L1, L2, and L5 signals of the GPS Block IIF satellites [25.105], which inhibit a proper exploitation of this method. This experience will grow with the advent of more signals and satellites, thus allowing a proper assessment of the different approaches.

25.3.4 Phase Ambiguity Fixing in PPP

Two principal benefits arise from fixing ambiguities to integers in the PPP context: improved positioning accuracy, specifically in the east component, and for filter-based PPP implementations, a reduction or possible elimination of the initial PPP solution convergence period. The latter benefit is particularly sought for the delivery of real-time PPP services, increasing their efficiency in achieving optimal solution accuracy.

DD phase ambiguity fixing has matured and is now routinely applied (Chap. 23) in either global or local positioning solutions. However, this is not directly applicable to PPP, due to the presence of pseudorange biases d and carrier-phase biases δ, which are eliminated in DD processing. This can be seen through a reparameterization of the basic observation model (25.1) explicitly exposing the different biases as follows

$$
\begin{aligned}
p^{\mathrm{s}}_{\mathrm{r,A}} &= \rho^{\mathrm{s}}_{\mathrm{r}} + c\,(dt_{\mathrm{r}} - dt^{\mathrm{s}}) + c\left(d_{\mathrm{r,A}} - d^{\mathrm{s}}_{\mathrm{A}}\right) \\
&\quad + T^{\mathrm{s}}_{\mathrm{r}} + I^{\mathrm{s}}_{\mathrm{r}} + e_{\mathrm{A}}\,, \\
p^{\mathrm{s}}_{\mathrm{r,B}} &= \rho^{\mathrm{s}}_{\mathrm{r}} + c\,(dt_{\mathrm{r}} - dt^{\mathrm{s}}) + c\left(d_{\mathrm{r,B}} - d^{\mathrm{s}}_{\mathrm{B}}\right) \\
&\quad + T^{\mathrm{s}}_{\mathrm{r}} + \mu I^{\mathrm{s}}_{\mathrm{r}} + e_{\mathrm{B}}\,, \\
\phi^{\mathrm{s}}_{\mathrm{r,A}} &= \rho^{\mathrm{s}}_{\mathrm{r}} + c\,(dt_{\mathrm{r}} - dt^{\mathrm{s}}) + c\left(\delta_{\mathrm{r,A}} - \delta^{\mathrm{s}}_{\mathrm{A}}\right) \\
&\quad + T^{\mathrm{s}}_{\mathrm{r}} - I^{\mathrm{s}}_{\mathrm{r}} + N_{\mathrm{A}}\lambda_{\mathrm{A}} + \epsilon_{\mathrm{A}}\,, \\
\phi^{\mathrm{s}}_{\mathrm{r,B}} &= \rho^{\mathrm{s}}_{\mathrm{r}} + c\,(dt_{\mathrm{r}} - dt^{\mathrm{s}}) + c\left(\delta_{\mathrm{r,B}} - \delta^{\mathrm{s}}_{\mathrm{B}}\right) \\
&\quad + T^{\mathrm{s}}_{\mathrm{r}} - \mu I^{\mathrm{s}}_{\mathrm{r}} + N_{\mathrm{B}}\lambda_{\mathrm{B}} + \epsilon_{\mathrm{B}}\,.
\end{aligned}
\tag{25.15}
$$

The measurement biases affecting undifferenced observations are functionally indistinguishable from the clock and ambiguity parameters. Disregarding them in PPP solutions, whether they originate from pseudorange or carrier phases, contaminates clocks and ambiguities. In recent years, much attention has been given by different research groups to resolve this issue [25.102, 106–113]. The proposed solutions require external information, in addition to the usual satellite

orbit/clock products, to break the link between biases and ambiguities and to restore the integer nature of the ambiguities. The proposed methods are largely equivalent as their differences lie primarily in the chosen parameterizations, in the way the rank deficiencies are eliminated and whether or not they make use of the ionosphere-free combined observations [25.11].

The decoupled clock model (DCM) described in [25.109, 114] combines the four observations of (25.15) into three combinations: the two ionosphere-free (IF) combined pseudoranges and carrier phases and the Melbourne–Wübenna combination (Chap. 20). The IF combined observations each have specific satellite and station clock parameters ($dt_{\mathrm{r},p_{\mathrm{IF}}}$, $dt^{\mathrm{s}}_{p_{\mathrm{IF}}}$, $dt_{\mathrm{r},\varphi_{\mathrm{IF}}}$, $dt^{\mathrm{s}}_{\varphi_{\mathrm{IF}}}$), which include the respective combined biases ($d_{\mathrm{r,IF}}$, $d^{\mathrm{s}}_{\mathrm{IF}}$, $\delta_{\mathrm{r,IF}}$, $\delta^{\mathrm{s}}_{\mathrm{IF}}$). The Melbourne–Wübenna combination is parameterized with the usual widelane-narrowlane (WL/NL) ambiguities and station and satellite WL biases ($d_{\mathrm{r,WL}}$; $d^{\mathrm{s}}_{\mathrm{WL}}$). All IF and WL biases are combinations of the original observation biases. In the DCM implementation, the integer nature of ambiguities is assured by fixing a minimum set of ambiguities to arbitrary integers (the ambiguity datum), while estimating the clock and bias parameters at discrete epochs. The N_{WL} and N_{NL} can then be resolved using common integer search schemes (Chap. 23). The additional satellite parameters required for PPP under DCM are, apart from the clock corrections, which now are pseudorange-specific and carrier-phase-specific, also satellite specific WL biases. The PPP algorithm must estimate two station clocks, one for each observation type, and a station WL bias. Finally, an ambiguity datum must be maintained within the PPP through a minimum set of ambiguities fixed to arbitrary integers.

The integer recovery clock (IRC) approach described in [25.115] uses the same base observation combinations (two IF and one WL), however the parameterization is slightly different: in addition to the satellite and station WL biases and ambiguous phase clocks, code-phase biases are defined, which can be likened to the difference of the DCM pseudorange specific and carrier-phase-specific clocks. In its implementation, the satellite WL biases are estimated as daily constants, while the station WL biases are estimated epoch per epoch, with a constraint on the overall mean. Similar to the DCM, the full system is defined by a subset of arbitrary integer ambiguities and the remaining WL-NL ambiguities are fixed in bootstrapping integer search algorithms. In practice, for both formulations found above, these arbitrary ambiguity data are constrained using the IF pseudoranges, so the ambiguous satellite and station carrier-phase clocks are somewhat consistent with the pseudorange-specific clocks.

Still other parameterizations than the above given ones are possible as well, like, for example, the common or distinct clock formulations of [25.102, 116]. As all methods provide intrinsically the same external information, one can establish their one-to-one transformations thus showing how the different methods can be mixed between networks and users [25.11]. Instead of the two IF clocks and one WL phase bias, for instance, as used by the DCM and IRC approaches, one can also base the required satellite parameters on the pseudorange-specific IF clock and two between satellite differenced NL-WL network ambiguities or two NL-WL uncalibrated carrier-phase delays [25.110–112].

In the uncalibrated phase delay (UPD) approach of [25.111] and [25.117], the station biases are eliminated through single differencing and the single-differenced UPDs are estimated modulo 1 (WL-NL) cycle. Similar to [25.115], the WL single-difference (SD)-UPDs are estimated as daily constants while the NL SD-UPDs are estimated as piecewise linear polynomials over specified intervals. These network-level products are computed for all satellite combinations, an appropriate selection of which must be matched in the PPP algorithms to provide SD constraints to undifferenced ambiguities.

Another PPP phase ambiguity fixing method, introduced by [25.118], uses DD carrier-phase ambiguities from network DD processing, which are reintroduced into the PPP algorithms as the condition equations of the new undifferenced observations. As it uses information from the global network solution, this method does not require a reparameterization of the observation equations and is very well suited for efficient back-substitution of global results into single station solutions.

In all the above models, PPP solutions require additional network-level products, such as decoupled clocks, pseudorange or carrier-phase biases or UPD/SD-UPDs, to isolate the integer value of ambiguities. However, further development is required to accelerate integer ambiguity resolution and reduce the period of initial convergence, the main operational issue in PPP. From pseudorange initialization at the half-meter to meter level, to the centimeter accuracy attained once all parameters have reached their optimal state, convergence may take 15 min and even longer, depending on receiver-specific pseudorange noise and on the local tracking environment (multipath, ionosphere, antenna dynamics, etc.).

Significant improvements (or even elimination) of PPP convergence is possible when external a priori ionospheric information can be provided. However, this requires precise knowledge of ionospheric delay variations, typically interpolated from local or regional

networks. Furthermore, one has to abandon the ionosphere-free combination approach and instead work with observables that are still sensitive to the ionospheric delays. This can be done, as demonstrated in [25.116, 119–122], by working with the four original measurement types of (25.15) without creating any linear combinations explicitly, or alternatively, as shown in [25.123], by replacing the ionosphere-free Melbourne–Wübbena combination by its carrier phase and pseudorange constituent parts. Note that such PPP algorithms with fixed atmospheric delays become equivalent to real-time kinematic (RTK), provided that a proper weighting of the observables (undifferenced, DD, or combined) is used [25.11].

Improved results were also shown when using observations made on more frequencies and/or when using more GNSS satellites [25.82, 124–127]. For more details on ambiguity resolution, see Chap. 23.

25.4 Implementations

The availability of global GNSS precise orbits and clocks from various sources has provided the opportunity to develop and implement PPP-based services for positioning and navigation. Post-processed PPP services for both static and kinematic positioning are proving to be particularly useful and efficient for reference frame densification. They have been adopted by several countries as an efficient way to supplement and reduce the expensive infrastructure of dense networks of geodetic monuments traditionally used to provide access to national geodetic reference frames. Internet-based post-processed PPP services are now offered by several institutions to fulfill that function (Chaps. 35 and 36). Many real-time (RT) PPP based positioning and navigation services have also emerged in recent years. RT PPP services are usually more costly to operate and tend to be offered commercially to specialized market segments such as agriculture or land and marine natural resources exploration and exploitation.

It may be useful here to distinguish between online positioning (and navigation) services based on PPP and those based on the differential approach. Although they may appear the same to users who need only to submit GNSS data from one station, they differ fundamentally in their implementation. Differential-based services such as the US National Geodetic Survey Opus and the GeoScience Australia AUSPOS need data from several stations to form the double differences required by their DD processing algorithm. This additional data is normally obtained from their national continuous operating reference stations (CORS) networks as well as from the IGS global network.

Reliance on data from one or more base stations in addition to the one provided by the users has both advantages and disadvantages. On the plus side, the differential services offer more robust cycle-slip detection and repair as well as simpler carrier-phase ambiguity fixing as long as a sufficient number of nearby stations are available. Failure to meet that condition quickly reduces the area of applicability of the differential technique. While the PPP method can be used globally with almost uniform performance, the differential approach is better suited to regional or continental applications. The remainder of this section will only cover PPP-based services. Irrespective of the specific method, positioning and their users benefit from the continuing standardization for exchange formats for GNSS observation data, the derived products and, to some extent, the resulting solutions (Annex A).

25.4.1 Post-Processed Solutions

Post-processed PPP services are usually more precise than their real-time counterparts and tend to be used for applications requiring accuracy and stability. Although not quite as precise as differential positioning over medium or short baselines (e.g., < 1000 km), post-processed PPP is rapidly being adopted in several regions to establish geodetic control (Chap. 36). This is especially true in remote areas where geodetic control monuments are sparsely distributed or nonexistent. Because of the stability of some of the GNSS orbits and clock products used, post-processed PPP is now providing long-term station velocity estimates for geodynamic applications that compare favorably with those obtained with the differential technique.

Typically for post-processed PPP applications, users submit GNSS data from a single station to the service via the Internet and receive, normally by e-mail and within minutes, an estimated position along with ancillary information. Depending on the service, various formats, such as RINEX, can be used for the GNSS data submission. Very little standardization currently exists for the dissemination of post-processed PPP results. Once received on the host server, GNSS data is processed according to the PPP method using GNSS orbits and clock corrections computed by the service provider or obtained from a third party such as the IGS. In addition to the orbits and clock corrections, PPP services may also call upon other specialized web services for additional corrections such as the ocean tide loading

corrections, troposphere delay parameters and receiver and satellite antenna PCVs.

In addition to the online services, PPP processing is now offered by several GNSS equipment manufacturers within their suite of post-processing software. The computations may be performed within a specialized PPP module or the GNSS data sent to an existing online service. In either case, results are seamlessly integrated into reports and other functions offered by those packages.

25.4.2 Real-Time Solutions

In contrast to the post-processed PPP services that rely on users sending GNSS observation data to a central server, most real-time applications require that GNSS orbit and clock corrections be sent in real time to the point of data collection. PPP position estimation is then performed according to PPP algorithms inside the GNSS receivers or on a colocated computer. Transmission of real-time corrections for PPP is usually done over the Internet using transport protocols developed for that purpose, such as NTRIP (networked transport of Radio Technical Commission for Maritime Services (RTCM) via Internet protocol [25.128]). To ensure that RT PPP services are available even in regions without access to high-speed Internet, some providers are also distributing corrections using geostationary communication satellites, which greatly increase service costs. Most real-time PPP services are currently offered for a cost by commercial enterprises. Costs of those services usually vary with the region as well as with the accuracy required.

Like post-processed PPP services, little standardization currently exists for RT PPP services as most are based on proprietary data formats and customized GNSS end-user equipment. Normally offered by providers of high-precision navigation services in niche markets, GNSS user equipment manufacturers or joint partnerships, RT PPP services tend to be closed-access and fully integrated services, where providers support end-to-end solutions, from computing real-time orbits and clock correction to embedding specialized software in end-user GNSS equipment. This could change in the coming years with the advent of new standardized formats applicable to RT PPP (Annex A) and Internet-based, free RT PPP corrections such as those of the IGS real-time service (Chap. 33). Open, real-time correction services, although useful for many applications, will require that algorithms in end-user applications be consistent with the models and conventions used to compute the correction streams.

25.4.3 PPP Positioning Services

Listing existing PPP based positioning services is problematic, since such a list can rapidly become outdated or incomplete. Nonetheless, a few examples of post-processed services often referenced in the literature are described in Table 25.3. The listed services all provide static or kinematic processing, use the RINEX observation format and output ITRF estimated coordinates. They, however, provide their results in nonstandard, service-specific output. Many of those services can be accessed and compared at Internet portals such as the University of New Brunswick's Precise Point Positioning Software Centre [25.129]. Other PPP services may exist that are specific to a given country, region or application.

Although each service has its own user interface, they should all provide comparable position estimates for a specific data set. A thorough assessment of the various services is, however, beyond the scope of this publication. For the interested reader, several papers comparing various post-processed and RT PPP services are available. Having several PPP services that provide independent position estimates also creates some redundancy and increases confidence that a PPP solution can be obtained whenever a particular service is unavailable or suspected of not providing reliable position estimates. However, caution is advised whenever comparing or integrating results from different services to ensure that estimated positions are for the same location, at the same epoch and in the same reference frame. Many services extract information directly from the observation file that is critical to identify the reference point of the position estimates, such as the receiver antenna type and antenna height. Processing reports should be closely examined to ensure that position estimates provided by the various services are indeed compatible.

Table 25.3 Post-processed PPP services

Service	URL	Provider
APPS	http://apps.gdgps.net/	Jet Propulsion Laboratory JPL (National Aeronautics and Space Administration NASA)
CSRS-PPP	http://webapp.geod.nrcan.gc.ca/geod/tools-outils/ppp.php	Natural Resources Canada
GAPS	http://gaps.gge.unb.ca/	University of New Brunswick
MAGIC GNSS	http://magicgnss.gmv.com/	GMV
Trimble RTX	http://www.trimblertx.com/	Trimble

25.5 Examples

To illustrate the performance offered by the precise point positioning concept, example results of GPS/GLONASS-based PPP solutions are presented in this section. The PPP software of Natural Resources Canada (NRCan; [25.130] and Table 25.3) has been used, along with 24 h data sets from 17 globally distributed IGS stations observed during the period of Jan. 1, 2012–Feb. 9, 2013. About half of the 17 stations are IGS reference frame stations, that is, a subset of those stations used to align IGS daily solutions to the current ITRF. To reduce computation time and also decrease possible correlation, 24 h PPP solutions using 5 min observation sampling were estimated at five-day intervals.

The NRCan PPP incorporates all the modeling effects described in Sect. 25.2, including ocean loading, higher-order ionospheric corrections, polar tides and a proper handling of eclipsing satellites for both GPS and GLONASS. However, the atmospheric and hydrological loading effects have not been applied here. Furthermore, only GMF and GPT have been used for tropospheric mapping and a priori ZTD_h, respectively, since GMF/GPT should give slightly better repeatability than the more rigorous VMF1 ones, when no atmospheric loading is applied (Sect. 25.2.1). Also, no ambiguity fixing (Sect. 25.3.4) has been employed. Although only the NRCan PPP software has been used here, other recent PPP implementations should give similar results.

25.5.1 Static PPP Solutions

Table 25.4 shows the comparison of static PPP positioning solutions with respect to IGS08 reference coordinates using final IGS GPS orbits/clock products as well as European Space Agency (ESA) GPS/GLONASS products. Note that Table 25.4 includes both mean offsets and repeatability of the daily static PPP solutions (one position solution for each 24 h interval), which are affected by real or apparent nonlinear station displacements during this 13-month period. Consequently, the RMS values (the last three columns of Table 25.4) are believed to be a good estimate of the accuracy of static PPP. Here one can notice that the addition of GLONASS has only slightly improved the RMS of the ESA GPS-only PPP solutions. This is likely due to small (real or apparent) systematic effects, common to both GPS and GLONASS PPP solutions. Nevertheless, even the accuracy of the ESA GLONASS-only PPP is quite impressive, considering that it is based on only 24 satellites and that the GLONASS orbit/clock modeling is still being improved.

As expected, the IGS final orbit/clock combinations yielded the smallest RMS of the mean offsets in Table 25.4, though the ESA GLONASS-only PPP RMSs were only slightly larger than the rest. The repeatability of IGS (GPS-only) and ESA GLONASS+GPS PPP solutions are the best. The GLONASS addition improved the longitude repeatability in particular, namely from 3.0 mm down to 2.7 mm.

Ambiguity fixing (Chap. 23), which was not been applied here, would also improve longitude repeatability to a level comparable to what is seen in latitude. The mean offset RMSs, on the other hand, are not expected to be improved by fixing ambiguities, as they are mainly due to station and orbit/clock systematic effects, which are not affected or reduced by ambiguity fixing. However, the initial PPP solution convergence, typically of about 15 min or longer for GPS-only PPP, may be significantly shortened when ambiguities are fixed (Sect. 25.3.4). This is not applicable here, since the 24 h PPP solutions are already fully converged, albeit to nonintegers.

Note that Table 25.4 includes some remote stations with suboptimal performance (e.g., OHI2, or the GLONASS HOB2 and DARW data), which have degraded repeatability and mean offset RMS. For most stations the repeatability and RMS are significantly better than those shown in Table 25.4 as can be seen from results previously shown in Fig. 25.3.

25.5.2 Kinematic PPP Solutions

In kinematic mode, independent PPP positions are estimated at each observation epoch, typically every 1–30 s, depending on application and user dynamics. When observation intervals are shorter than the satellite clock sampling, clock interpolation is necessary. Due to satellite clock instability, only clocks at 30 s or lower sampling interval can be reliably interpolated at the cm precision level. IGS and most IGS AC clock solutions currently use 30 s sampling but higher-rate clock products may be offered by individual analysis centers for specific applications [25.131].

To demonstrate kinematic PPP performance, even though under rather ideal conditions, the 17-station static dataset discussed before has also been reprocessed in kinematic mode, where an independent position is solved at each observation (and satellite clock) epoch. Since backward smoothing (substitution) was used for all kinematic PPP solutions, the statistics reflect the solution quality after ambiguity convergence. The resulting kinematic PPP epoch repeatability for each of the 17 stations with the final IGS (GPS-only)

Table 25.4 Repeatability and root mean square (RMS) of the static daily PPP mean offsets (in mm) with respect the IGS08 positions at 17 globally distributed IGS stations, between Jan. 1, 2012 and Feb. 9, 2013, obtained with the final IGS GPS and ESA AC GLONASS/GPS orbits/clocks. Columns dN, dE, and dH refer to the north (latitude), east (longitude) and height (up) component of the position

Static PPP	σ			RMS of means			RMS		
AC orbits/clocks	dN (mm)	dE (mm)	dH (mm)	dN (mm)	dE (mm)	dH (mm)	dN (mm)	dE (mm)	dH (mm)
igs (GPS)	2.2	3.2	6.6	1.7	2.2	3.6	2.8	3.9	7.5
esa (GPS)	2.3	3.0	6.6	2.9	2.3	3.7	3.7	3.8	7.6
esa (GLONASS)	2.4	3.3	7.7	3.0	3.0	4.2	3.8	4.5	8.8
esa (GLONASS+GPS)	2.2	2.7	6.6	2.8	2.5	3.7	3.6	3.7	7.6

and ESA (both GPS and GLONASS) orbits/clocks are shown in Table 25.5.

As expected, the ESA GLONASS+GPS kinematic PPP performed the best, better than GPS-only PPP using the IGS or ESA orbits/clocks. The latitude and longitude of the GLONASS+GPS PPP solutions have sub-cm repeatability at most stations, while the height repeatability is about twice as large (i. e., 2 cm or less at most stations). Note that the RMS differences with respect to IGS08 (not shown here) are about the same as the static PPP RMS, which are much smaller than the kinematic PPP repeatability. Consequently, kinematic PPP repeatability can be seen to represent post-processed kinematic PPP accuracy, achievable under ideal observing conditions (static).

The GLONASS-only kinematic PPP solutions in Table 25.5 performed much worse than the GPS-only ones, with repeatability often exceeding 5 cm. This should be expected, as there are only 24 GLONASS satellites, yielding weaker geometry and less robust epoch solutions than the 32 GPS satellites. Furthermore, GLONASS orbits/clocks are still less precise and less robust than the GPS ones. Nevertheless, adding GLONASS data already improves kinematic PPP precision or accuracy, sometimes quite significantly. Even for several remote stations (e.g., DARW and HOB2), which had rather large sigmas for GLONASS-only PPP repeatability (Table 25.5), the addition of GLONASS data improved in most cases the GPS-only PPP, sometimes quite significantly. In a real dynamic environment, users are cautioned that kinematic PPP precision can be considerably worse, in particular when operating in real time, which cannot take the advantage of post processing and backward smoothing and is impacted by additional errors due to latencies of real-time clock solutions.

Table 25.5 Repeatability (σ [cm]) of kinematic PPP solutions at 17 IGS stations with IGS and ESA orbit clock products using GPS-only (G), GLONASS-only (R) and GPS+GLONASS (GR) observations (Jan. 1, 2012–Feb. 9, 2013)

Station	North				East				Up			
	IGS G	ESA G	ESA R	ESA RG	IGS G	ESA G	ESA R	ESA RG	IGS G	ESA G	ESA R	ESA RG
CHUR	1.9	1.2	1.8	1.0	2.9	1.4	2.3	0.9	3.8	2.7	3.3	1.5
VALD	0.8	0.9	2.9	1.1	1.0	1.1	4.2	0.8	2.0	2.0	10.9	1.5
WHIT	1.4	1.2	9.2	0.7	1.4	1.4	3.5	0.7	2.6	2.5	14.4	1.4
GOLD	0.8	7.4	71.9	0.7	1.0	16.2	211.9	0.7	2.6	12.9	213.3	1.8
HOFN	1.5	1.3	1.8	0.6	1.1	1.1	3.2	0.5	2.7	2.4	4.5	1.4
ONSA	0.8	0.9	0.9	0.6	0.7	0.7	1.1	0.5	2.2	1.9	2.6	1.4
WTZR	1.0	1.1	1.4	0.7	1.0	1.7	4.2	0.7	2.3	3.3	5.7	1.6
OB2	1.0	1.1	20.7	0.9	1.1	1.2	44.5	1.0	2.9	2.5	169.2	2.0
DARW	1.0	1.1	804.3	1.0	1.3	1.4	981.0	1.5	3.1	3.8	4452	3.0
CHTI	0.8	0.9	1.3	0.6	0.9	1.0	2.1	0.7	2.3	2.1	3.3	1.6
MAW1	2.3	4.3	5.4	0.7	2.6	5.8	8.4	0.6	4.7	4.0	9.6	1.4
HARB	1.1	1.0	1.8	0.8	1.0	1.4	3.1	1.0	2.6	2.7	4.2	2.1
GUUG	1.5	1.7	8.0	1.3	1.8	2.0	14.4	1.5	4.7	5.7	16.6	3.9
GMSD	0.9	1.0	1.5	0.7	1.0	1.1	2.8	0.8	2.8	2.7	5.0	2.1
KOKV	1.8	1.5	18.0	0.7	1.5	1.9	23.7	1.0	3.4	9.0	14.8	2.8
CONZ	0.8	1.0	4.6	0.6	1.0	1.4	7.6	0.9	2.6	2.5	11.4	1.8
OHI2	1.0	1.0	0.9	0.7	1.1	1.1	1.0	0.7	2.2	2.2	2.2	1.6
RMS	1.27	2.34	196	0.81	1.44	4.36	243.78	0.90	3.01	4.75	1082	2.05

25.5.3 Tropospheric Zenith Path Delay

Another parameter estimate available in a PPP solution is the wet tropospheric zenith path delay ZTD_w, which when added to the a priori hydrostatic ZTD_h, yields the total ZTD. When the wet and dry ZTD and the corresponding mapping functions are properly separated (Sect. 25.2.1), ZTD_w can be used to infer the atmospheric precipitable water content (Chap. 38), which can be assimilated into a NWM, although the total ZTD is usually preferred.

Figure 25.4 gives an example of total ZTD PPP solutions at the former IGS station CHAT obtained in 2009 (with an earlier version of the NRCan PPP software), utilizing the IGS Final GPS orbits/clocks. The PPP also estimated stochastic ZTD gradient solutions (Sect. 25.2.1), which are rather small and for brevity are not shown here. The PPP solutions (at 5 min sampling) are compared to the IGS total ZTD products, which are also using 5 min sampling and IGS orbit/clock PPP, but are generated with a different software (GIPSY/OASIS [25.132]). Figure 25.4 also compares the ZTD of the CODE AC, GFZ AC and JPL AC global solutions with the IGS ZTD products. One can see a fairly good agreement for all ZTD solutions, which use the 5 min sampling (IGS, JPL, PPP). The 0.5 h and 2 h samplings, used respectively by GFZ and CODE, are not as responsive to the rapid changes of the total ZTD in the second half of the week (see the ZTD scale on the right). They have likely caused the fairly large (COD-IGS) and (GFZ-IGS) ZTD differences.

The same comparisons seen in Fig. 25.4 have also been done at 33 globally distributed IGS reference stations resulting in a RMS of 2.8 mm for the (PPP-IGS) ZTD differences. ZTD solutions based on the current PPP software version and the latest IGS orbit/clock and ZTD solutions should give an even better agreement. It is important to realize that the ZTD and height PPP parameters are weakly correlated, namely up to 20% of height errors (either real or apparent) may be mapped into ZTD estimates [25.133]. This is why it is essential that for precise ZTD solutions all the models of Sect. 25.2 be properly taken into account.

25.5.4 Station Clock Solutions

Time and frequency transfer applications of GNSS will be addressed specifically in Chap. 41. This section shows the level of precision at which station clock parameters are recovered using PPP. For this purpose, eight IGS stations (AMC2, BRUX, IENG, NRC1, PTBB, SPT0, USN3, WAB2) located at time and frequency laboratories were processed in three successive 24 h PPP solutions using the NRCan-PPP software in static mode and applying backward smoothing (substitution) to eliminate the initial convergence period. IGS final satellite orbit and clock products were used. The IGS clock products also include stations clock estimates that are consistent with those of satellites, all clocks being referenced to the IGS timescale [25.134].

Figure 25.5 shows the difference of PPP station clock estimates with respect to the IGS Final solutions, where the level of agreement is a few 100 ps (equivalent to 3 cm) or less for the best performing stations, and the solution boundary discontinuities are typical of the systematic effect of pseudorange errors averaged over the 24 h solution interval.

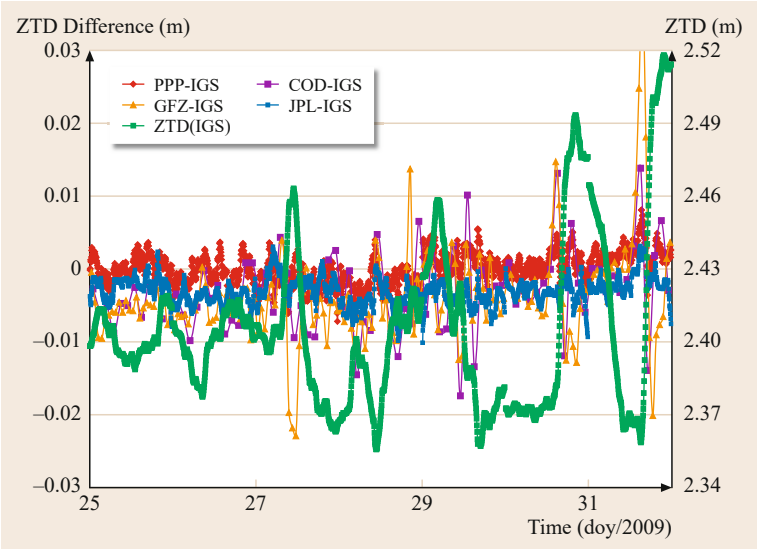

Fig. 25.4 Total ZTD differences from PPP with IGS final orbits/clocks (PPP-IGS) along with Center for Orbit Determination in Europe (CODE), Deutsches GeoForschungsZentrum Potsdam (GFZ) and JPL analysis center solutions with respect to IGS total ZTD at the former IGS station CHAT. The RMS of PPP-IGS ZTD differences are 2.3 mm for station CHAT during this week-long period and 2.8 mm for 33 globally distributed IGS reference stations (IGS, PPP and JPL used 5 min ZTD solution sampling; GFZ and CODE AC used 0.5 h and 2 h ZTD solution intervals, respectively) (after [25.65])

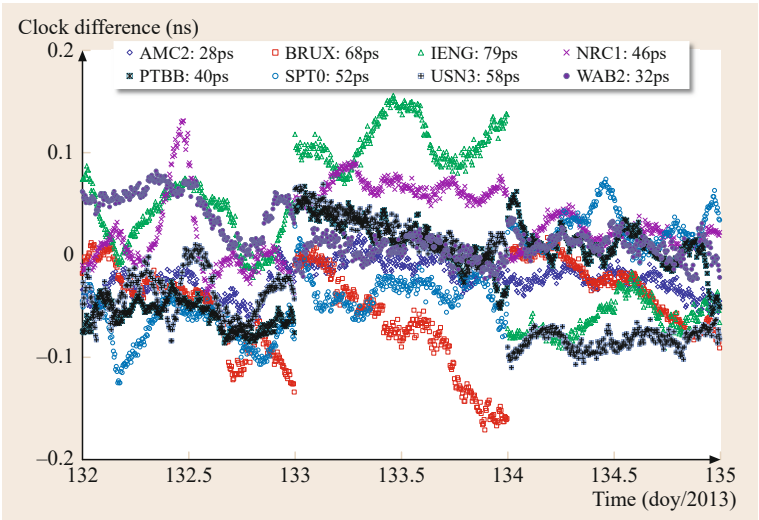

Fig. 25.5 Daily PPP clock solution differences with respect to IGS final solutions for eight IGS stations located at time and frequency laboratories for three consecutive days. RMS differences for each station are below 200 ps

25.6 Discussion

The dual-frequency PPP concept, with related methodology and modeling for static and kinematic PPP solutions with respective precisions of a few mm and one cm, has been reviewed and discussed. Such PPP solutions include position estimates that are directly in the reference frame of the input orbits/clocks, but also facilitate consistent recovery of ZTD solutions at a few-mm level and station clock solutions at the subnanosecond level. Even in single-frequency mode, using ionosphere-free code-plus-phase combinations enables a fairly precise kinematic PPP (navigation) at a few-dm level. This single-frequency PPP can also facilitate ionospheric total electron content (TEC) solutions and monitoring, which compare favorably with the ones based on dual-frequency pseudorange observations.

The PPP solutions can be viewed as an efficient means of realizing the reference frame implied by the fixed orbits/clocks. In fact, they are a station-based back substitution of the global network solutions applied to generate the orbits/clocks products. Consequently, dual-frequency PPP position, ZTD and clock solutions should be as precise as the ones obtained in the corresponding global solutions, provided that the PPP uses consistent models and ambiguity fixing. Ambiguity fixing can improve the PPP positioning precision, particularly the longitude solutions using data spans significantly shorter than 24 h, and it can possibly reduce the time period to initial PPP solution convergence, or even eliminate it, if external, precise ionospheric delays are available.

Even though the above discussions and review pertained mainly to the dual-frequency (L1, L2) PPP with GPS and GLONASS orbits/clocks, extension to a different frequency pair (e.g., L1, E5) and emerging GNSS constellations, such as BeiDou ad Galileo, are straightforward, once all intersystem biases are resolved. Addition of new GNSS signals and satellites will be quite beneficial to PPP solutions, making them more precise and robust, particularly so for kinematic applications. In fact, independent PPP processing of observations from different GNSS systems may provide the redundancy required to facilitate the evaluation of geodetic quantities, as new observation combinations and orbital geometries are exploited to analyze local and long-term systematic effects.

The above discussions have relied heavily on IGS developed conventions (modeling and formats) and IGS orbit/clock products. It is likely that developers and users of PPP will use the IGS orbit/clock solutions, in particular when long time series are to be analyzed with the highest accuracy for consistency with the current IERS standards. It is encouraging to know that the IGS mandate also calls for the provision of orbit/clock solutions for all available GNSSs, as they emerge. Despite their IGS focus, the above discussions should also benefit PPP users of other, for example commercial orbit/clock services, since most of these services benefit from and largely follow the IGS modeling, conventions and developments.

Without IERS conventions and readily available IGS products [25.135] resulting from the significant efforts sustained to develop precise orbit models by many participating organizations, efficient and precise PPP solutions such as those discussed here would not have

been possible. PPP solutions can only be as accurate as implied by the adopted GNSS orbits and clocks!

Acknowledgments. Data and solution products from the International GNSS Service (IGS) have been used in the preparation of this chapter. Also, the significant help and contributions of the Editors, Oliver Montenbruck and Peter Teunissen, are acknowledged, in particular in regards to the emerging GNSS signals and undifferenced ambiguity resolutions.

References

25.1 J.D. Bossler, C.C. Goad, P.L. Bender: Using the global positioning system (GPS) for geodetic positioning, Bull. Geod. **54**, 101–114 (1980)

25.2 J.F. Zumberge, M.B. Heflin, D.C. Jefferson, M.M. Watkins, F.H. Webb: Precise point positioning for the efficient and robust analysis of GPS data from large networks, J. Geophys. Res. **102**, 5005–5017 (1997)

25.3 S. Bisnath, Y. Gao: Current state of precise point positioning and future prospects and limitations. In: *Observing Our Changing Earth*, ed. by M.G. Sideris (Springer, Berlin 2009) pp. 615–623

25.4 S. Banville, R. Langley: Mitigating the impact of ionospheric cycle slips in GNSS observations, J. Geodesy **87**, 179–193 (2013)

25.5 R. Schmid, P. Steigenberger, G. Gendt, M. Gendt, M. Rothacher: Generation of a consistent absolute phase center correction model for GPS receiver and satellite antennas, J. Geodesy **81**(12), 781–798 (2007)

25.6 O. Montenbruck, R. Schmid, F. Mercier, P. Steigenberger, C. Noll, R. Fatkulin, S. Kogure, S. Ganeshan: GNSS satellite geometry and attitude models, Adv. Space Res. **56**(6), 1015–1029 (2015)

25.7 G.P.S. Directorate: *Navstar GPS Space Segment / Navigation User Segment Interfaces, Interface Specification, IS-GPS-200H, 24 Sep. 2013* (Global Positioning Systems Directorate, Los Angeles Air Force Base, El Segundo 2013)

25.8 J. Kouba: Improved relativistic transformations in GPS, GPS Solutions **8**(3), 170–180 (2004)

25.9 S. Schaer: Overview of GNSS biases, Proc. workshop on GNSS biases, Univ., Bern (2012), (2012)

25.10 O. Montenbruck, A. Hauschild, P. Steigenberger: Differential code bias estimation using multi-GNSS observations and global ionosphere maps, Navigation **61**(3), 191–201 (2014)

25.11 P.J.G. Teunissen, A. Khodabandeh: Review and principles of PPP-RTK methods, J. Geodesy **89**(3), 217–240 (2015)

25.12 O. Bock, E. Doerflinger: Atmospheric modeling in GPS data analysis for high accuracy positioning, Phys. Chem. Earth Part A **26**(6), 373–383 (2001)

25.13 G. Petit, B. Luzum: *IERS Conventions (2010)*, IERS Technical Note No. 36 (Verlag des Bundesamts für Kartographie und Geodäsie, Frankfurt 2010)

25.14 J. Boehm, A. Niell, P. Tregonning, H. Schuh: Global mapping function (GMF): A new empirical mapping function based on numerical weather model data, Geophys. Res. Lett. **33**(L07304), 1–4 (2006)

25.15 J. Boehm, P. Heinkelmann, H. Schuh: Short note: A global model of pressure and temperature for geodetic applications, J. Geodesy **81**(10), 679–683 (2007)

25.16 M. Hernández-Pajares, J.M. Juan, J. Sanz, R. Orus, A. Garcia-Rigo, J. Feltens, A. Komjathy, S.C. Schaer, A. Krankowski: The IGS VTEC maps: A reliable source of ionospheric information since 1998, J. Geodesy **83**(3/4), 263–275 (2009)

25.17 M.M. Hoque, N. Jakowski: Higher order ionospheric effects in precise GNSS positioning, J. Geodesy **81**(4), 259–268 (2007)

25.18 Z. Altamimi, L.T. Métivier, X. Collilieux: ITRF2008 plate motion model, J. Geophys. Res. **117**(B07402), 1–14 (2012)

25.19 P.M. Mathews, V. Dehant, J.M. Gipson: Tidal station displacements, J. Geophys. Res. **102**(B9), 20469–20477 (1997)

25.20 S.A. Melachroinos, R. Biancale, M. Llubes, F. Perosanz, F. Lyard, M. Vergnolle, M.-N. Bouin, F. Masson, J. Nicolas, L. Morel, S. Durand: Ocean tide loading (OTL) displacements from global and local grids: Comparisons to GPS estimates over the shelf of Brittany, France, J. Geodesy **82**(6), 357–371 (2008)

25.21 M.A. King, Z. Altamimi, J. Boehm, M. Bos, R. Dach, P. Elosegui, F. Fund, M. Hernández-Pajares, D. Lavallee, P.J. Mendes Cerveira, N. Penna, R.E.M. Riva, P. Steigenberger, T. van Dam, L. Vittuari, S. Williams, P. Willis: Improved constraints on models of glacial isostatic adjustment: A review of the contribution of ground-based geodetic observations, Surveys Geophys. **31**(5), 465–507 (2010)

25.22 T. van Dam, X. Collilieux, J. Wuite, Z. Altamimi, J. Ray: Nontidal ocean loading: Amplitudes and potential effects in GPS height time series, J. Geodesy **86**(11), 1043–1057 (2012)

25.23 L. Petrov, J.-P. Boy: Study of the atmospheric pressure loading signal in very long baseline interferometry observations, J. Geophys. Res. **109**(B03405), 1–14 (2004)

25.24 B. Görres, J. Campbell, M. Becker, M. Siemes: Absolute calibration of GPS antennas: Laboratory results and comparison with field and robot techniques, GPS Solutions **10**(2), 136–145 (2006)

25.25 J.T. Wu, S.C. Wu, G.A. Hajj, W.I. Bertiger, S.M. Lichten: Effects of antenna orientation on GPS carrier-phase, Man. Geodetica **18**, 91–98 (1993)

25.26 A.Q. Le, C.C.J.M. Tiberius: Phase wind-up effects in precise point positioning with kinematic platforms, Proc. NAVITEC, Noordwijk (2006) pp. 1–8, (ESA, Noordwijk 2006)

25.27 P. Steigenberger: Accuracy of Current and Future Satellite Navigation Systems, Habilitation Thesis (Fakultät Bau Geo Umwelt, Technische Universität München, Munich 2015)

25.28 W.M. Folkner, J.G. Williams, D.H. Boggs: *The Planetary and Lunar Ephemeris DE421*, Memorandum IOM 343R-08-003 (Jet Propulsion Laboratory, Pasadena 2008)

25.29 J.L. Hilton, C.Y. Hohenkerk: A comparison of the high accuracy planetary ephemerides DE421, EPM2008, and INPOP08, Proc. Journées, 2010, "Systèmes de Réfrence Spatio-Temporels" (JSR2010): New challenges for reference systems and numerical standards in astronomy, Paris, ed. by N. Capitaine (Observatoire de Paris, Paris 2011) pp. 77–80

25.30 H.F. Fliegel, K.M. Harrington: Sun/Moon position routines for GPS trajectory calculations, Proc. AIAA/AAS Astrodyn. Conf., Hilton Head Island (1992) pp. 625–631

25.31 J.H. Meeus: *Astronomical Algorithms* (Willmann-Bell, Richmond 1991)

25.32 O. Montenbruck, E. Gill: *Satellite Orbits – Models, Methods and Applications* (Springer, Berlin 2000)

25.33 H.A. Marques, J.F.G. Monico, M. Aquino: RINEX_HO: Second-and third-order ionospheric corrections for RINEX observation files, GPS Solutions **15**(3), 305–314 (2011)

25.34 N. Jakowski, F. Porsch, G. Mayer: Ionosphere-induced-ray-path bending effects in precise satellite positioning systems, Z. Satell. Position. Navig. Kommun. **SPN 1/94**, 6–13 (1994)

25.35 Z. Wang, Y. Wu, K. Zhang, Y. Meng: Triple-frequency method for high-order ionospheric refractive error modelling in GPS modernization, J. Glob. Position. Syst. **1**(9), 291–295 (2005)

25.36 J. Saastamoinen: Atmospheric correction for the troposphere and stratosphere in radio ranging of satellites. In: *The Use of Artificial Satellites for Geodesy*, Geophysical Monograph, Vol. 15, ed. by S.W. Henriksen, A. Mancini, B.H. Chovitz (AGU, Washington 1972) pp. 247–251

25.37 J.L. Davis, T.A. Herring, I.I. Shapiro, A.E.E. Rogers, G. Elgered: Geodesy by radio interferometry: Effects of atmospheric modeling errors on estimates of baseline length, Radio Sci. **20**(6), 1593–1607 (1985)

25.38 G. Chen, T.A. Herring: Effects of atmospheric azimuthal asymmetry on the analysis of space geodetic data, J. Geophys. Res. **102**(B9), 20489–20502 (1997)

25.39 D.S. MacMillan, C. Ma: Atmospheric gradients and the VLBI terrestrial and celestial reference frames, Geophys. Res. Lett. **24**(4), 453–456 (1997)

25.40 J.W. Marini: Correction of satellite tracking data for an arbitrary tropospheric profile, Radio Sci. **7**(2), 223–231 (1972)

25.41 K.M. Lagler, M. Schindelegger, J. Bohm, H. Krasna, T. Nilsson: GPT2: Empirical slant delay model for radio space geodetic techniques, Geophys. Res. Lett. **40**(6), 1069–1073 (2013)

25.42 J. Boehm, B. Werl, H. Schuh: Troposphere mapping functions for GPS and very long baseline interferometry from European centre for medium-range weather forecasts operational analysis data, J. Geophys. Res. **111**(B02406), 1–9 (2006)

25.43 L. Urquhart, F.G. Nievinski, M.C. Santos: Assessment of troposphere mapping functions using three dimensional raytracing, GPS Solutions **18**(3), 345–354 (2014)

25.44 *GGOS Atmosphere – Atmosphere Delays* (Vienna Univ. Technology, Vienna 2014) http://ggosatm.hg.tuwien.ac.at/delay.html

25.45 *UNB Vienna Mapping Function Service* (Univ. New-Brunswick, Frederiction 2015) http://unb-vmf1.gge.unb.ca/

25.46 J. Kouba: Implementation and testing of the gridded Vienna mapping function 1 (VMF1), J. Geodesy **82**, 193–205 (2008)

25.47 J. Kouba: Testing of global pressure/temperature (GPT) model and global mapping function (GMF) in GPS analyses, J. Geodesy **83**(3), 199–208 (2009)

25.48 R. Schmid: Upcoming switch to IGS08/igs08.atx – Details on igs08.atx (IGS Mail 6355; International GNSS Service, 7 Mar. 2011) http://igscb.jpl.nasa.gov/pipermail/igsmail/2011/006347.html

25.49 G. Wübbena, M. Schmitz, G. Boettcher, C. Schumann: Absolute GNSS antenna calibration with a robot: Repeatability of phase variations, calibration of GLONASS and determination of carrier-to-noise pattern, Proc. IGS Workshop, Darmstadt (ESA/ESOC, Darmstadt 2006) pp. 1–12

25.50 RINEX – The Receiver Independent Exchange Format – Version 3.03 14 July 2015 (IGS RINEX WG and RTCM-SC104, 2015)

25.51 L. Scott: Why do GNSS systems use circular polarization antennas?, Inside GNSS **2**(2), 30–33 (2007)

25.52 M.L. Psiaki, S. Mohiuddin: Modeling, analysis, and simulation of GPS carrier phase for spacecraft relative navigation, J. Guid. Contr. Dyn. **30**(6), 1628–1639 (2007)

25.53 Y.E. Bar-Sever: A new module for GPS yaw attitude control, Proc. IGS Workshop – Special Topics and New Directions, Potsdam (GeoforschungsZentrum, Potsdam 1996) pp. 128–140

25.54 J. Kouba: A simplified yaw-attitude model for eclipsing GPS satellites, GPS Solutions **13**(1), 1–12 (2009)

25.55 F. Dilssner, R. Springer, G. Gienger, J. Dow: The GLONASS-M satellite yaw-attitude model, Adv. Space Res. **47**(1), 160–171 (2010)

25.56 S. Banville, H. Tang: Antenna rotation and its effects on kinematic precise point positioning, Proc. ION GNSS 2010, Portland (ION, Virginia 2010) pp. 2545–2552

25.57 D.D. McCarthy: *IERS Conventions (1989)*, IERS Technical Note No. 3 (Observatoire de Paris, Paris 1989)

25.58 J.M. Wahr: The forced nutation of an elliptical, rotating, elastic, and ocean less Earth, Geophys.

J. R. Astron. Soc. **64**, 705–727 (1981)
25.59 G. Jentzsch: Earth tides and ocean tidal loading. In: *Tidal Phenomena*, ed. by H. Wilhelm, H.G.W. Wenzel Zürn (Springer, Berlin 1997) pp. 145–171
25.60 H. Dragert, T.S. James, A. Lambert: Ocean loading corrections for continuous GPS: A case study at the Canadian coastal site holberg, Geophys. Res. Lett. **27**(14), 2045–2048 (2000)
25.61 H.G. Scherneck: A parameterized solid earth tide model and ocean tide loading effects for global geodetic baseline measurements, Geophs. J. Int. **106**, 677–694 (1991)
25.62 Online ocean tide loading computation service (Chalmers University) http://holt.oso.chalmers.se/loading/
25.63 O. Montenbruck, A. Hauschild: Code biases in multi-GNSS point positioning, Proc. ION ITM 2013, San Diego (ION, Virginia 2013) pp. 616–628
25.64 O. Montenbruck, P. Steigenberger, R. Khachikyan, G. Weber, R.B. Langley, L. Mervart, U. Hugentobler: IGS-MGEX: Preparing the ground for multi-constellation GNSS science, Inside GNSS **9**(1), 42–49 (2014)
25.65 J. Kouba: *A Guide to Using International GNSS Service (IGS) Products* (IGS, Pasadena 2015), http://kb.igs.org/
25.66 International GNSS Service: Analysis center information ftp://igscb.jpl.nasa.gov/igscb/center/analysis/
25.67 R.R. Hatch: The synergism of GPS code and carrier measurements, Proc. Third Int. Geodetic Symp. Satellite Doppler Positioning, Las Cruces (Physical Science Laboratory, Las Cruces 1982) pp. 1213–1232
25.68 O. Øvstedal: Absolute positioning with single-frequency GPS receivers, GPS Solutions **5**(4), 33–44 (2002)
25.69 A.Q. Le, C. Tiberius: Single-frequency precise point positioning with optimal filtering, GPS Solutions **11**(1), 61–69 (2007)
25.70 R.J.P. van Bree, C.C.J.M. Tiberius: Real-time single-frequency precise point positioning: Accuracy assessment, GPS Solutions **16**(2), 259–266 (2012)
25.71 A. Tetewsky, J. Ross, A. Soltz, N. Vaughn, J. Anzperger, Ch. O'Brien, D. Graham, D. Craig, J. Lozow: Making sense of inter-signal corrections – Accounting for GPS satellite calibration parameters in legacy and modernized ionosphere correction algorithms, Inside GNSS **4**(4), 37–48 (2009)
25.72 P. Héroux, J. Kouba: GPS precise point positioning with a difference, Geomatics'95, Ottawa (1995) pp. 1–11
25.73 T.P. Yunck: Coping with the atmosphere and ionosphere in precise satellite and ground positioning. In: *Environmental Effects on Spacecraft Positioning and Trajectories*, ed. by A.V. Jones (AGU, Washington 1992), Chap. 1, pp. 1–16
25.74 H. Van Der Marel, P. De-Bakker: Single versus dual-frequency precise point positioning – What are the tradeoffs between using L1-only and L1+L2 for PPP?, Inside GNSS **7**(4), 30–35 (2012)
25.75 S. Choy, K. Zhang, D. Silcock: An evaluation of various ionospheric error mitigation methods used in single frequency PPP, J. Glob. Position. Syst. **7**(1), 62–71 (2008)
25.76 T. Schüler, H. Diessongo, Y. Poku-Gyamfi: Precise ionosphere-free single-frequency GNSS positioning, GPS Solutions **15**(2), 139–147 (2011)
25.77 H.T. Diessongo, H. Bock, T. Schüler, S. Junker, A. Kiroe: Exploiting the Galileo E5 wideband signal for improved single-frequency precise positioning, Inside GNSS **7**(5), 64–73 (2012)
25.78 K. Chen, Y. Gao: Real-time precise point positioning using single frequency data, Proc. ION GNSS 2005, Long Beach (2005), pp. 1514 –1523
25.79 S. Banville, R.B. Langley: Cycle-slip correction for single-frequency PPP, Proc. ION GNSS 2012, Nashville (ION, Virginia 2012) pp. 3753–3761
25.80 C. Cai, Y. Gao: Precise point positioning using combined GPS and GLONASS observations, J. Glob. Position. Syst. **6**(1), 13–22 (2007)
25.81 L. Wanninger, S. Wallstab-Freitag: Combined processing of GPS, GLONASS, and SBAS code phase and carrier phase measurements, Proc. ION GNSS 2007, Fort Worth (ION, Virginia 2007) pp. 866–875
25.82 C. Cai, Y. Gao: Modeling and assessment of combined GPS/GLONASS precise point positioning, GPS Solutions **17**(4), 223–236 (2013)
25.83 T. Melgard, E. Vigen, O. Orpen: Advantages of combined GPS and GLONASS PPP – Experiences based on G2, a new service from Fugro, Proc. 13th IAIN World Congress, Stockholm (IAIN, London 2009) pp. 1–7
25.84 S. Choy, S. Zhang, F. Lahaye, P. Héroux: A comparison between GPS-only and combined GPS+GLONASS precise point positioning, J. Spatial Sci. **58**(2), 169–190 (2013)
25.85 L. Wanninger: Carrier-phase inter-frequency biases of GLONASS receivers, J. Geodesy **86**(2), 139–148 (2012)
25.86 J.M. Sleewaegen, A. Simsky, W. Boon, F. de Wilde, T. Willems: Demystifying GLONASS inter-frequency carrier-phase biases, Inside GNSS **7**(3), 57–61 (2012)
25.87 M. Becker, P. Zeimetz, E. Schönemann: Anechoic chamber calibrations of phase center variations for new and existing GNSS signals and potential impacts in IGS processing, Proc. IGS Workshop, Newcastle (IGS, Pasaden 2010) pp. 1–44
25.88 P. Steigenberger, U. Hugentobler, S. Loyer, F. Perosanz, L. Prange, R. Dach, M. Uhlemann, G. Gendt, O. Montenbruck: Galileo orbit and clock quality of the IGS multi-GNSS experiment, Adv. Space Res. **55**(1), 269–281 (2015)
25.89 Y. Lou, Y. Liu, C. Shi, X. Yao, F. Zheng: Precise orbit determination of BeiDou constellation based on BETS and MGEX network, Sci. Rep. **4**(4692), 1–10 (2014)
25.90 P. Steigenberger, A. Hauschild, O. Montenbruck, C. Rodriguez-Solano, U. Hugentobler: Orbit and clock determination of QZS-1 based on the CONGO network, Navigation **60**(1), 31–40 (2013)

25.91 L. Prange, E. Orliac, R. Dach, D. Arnold, G. Beutler, S. Schaer, A. Jäggi: CODE's multi-GNSS orbit and clock solution, Proc. EGU General Assembly, Vienna (EGU, Munich 2015) p. 11494

25.92 J. Tegedor, O. Øvstedal, E. Vigen: Precise orbit determination and point positioning using GPS, Glonass, Galileo and BeiDou, J. Geod. Sci. **4**(1), 65–73 (2014)

25.93 D. Odijk, P.J.G. Teunissen: Characterization of between-receiver GPS-Galileo inter-system biases and their effect on mixed ambiguity resolution, GPS Solutions **17**(4), 521–533 (2013)

25.94 D. Odijk, P.J.G. Teunissen: Estimation of differential inter-system biases between the overlapping frequencies of GPS, Galileo, BeiDou and QZSS, Proc. 4th Int.Coll. Scientific and Fundamental Aspects of the Galileo Programme, Prague 2013 (ESA, Noordwijk 2013) pp. 1–8

25.95 A. Dalla Torre, A. Caporali: An analysis of intersystem biases for multi-GNSS positioning, GPS Solutions **19**(2), 297–307 (2015)

25.96 J. Paziewski, P. Wielgosz: Accounting for Galileo–GPS inter-system biases in precise satellite positioning, J. Geodesy **89**(1), 81–93 (2015)

25.97 H. Cui, G. Tang, S. Hu, B. Song, H. Liu, J. Sun, P. Zhang, C. Li, M. Ge, C. Han: Multi-GNSS processing combining GPS, GLONASS, BDS and GALILEO observations, Proc. CSNC, Nanjing, Vol. III (2014), ed. by J. Sun, W. Jiao, H. Wu, M. Lu (Springer, Berlin 2014) pp. 121–132

25.98 X. Li, X. Zhang, X. Ren, M. Fritsche, J. Wickert, H. Schuh: Precise positioning with current multi-constellation global navigation satellite systems: GPS, GLONASS, Galileo and BeiDou, Sci. Rep. **5**(8328), 1–14 (2015)

25.99 X. Li, M. Ge, X. Dai, X. Ren, M. Fritsche, J. Wickert, H. Schuh: Accuracy and reliability of multi-GNSS real-time precise positioning: GPS, GLONASS, BeiDou, and Galileo, J. Geodesy **89**(6), 607–635 (2015)

25.100 P.J.G. Teunissen, R. Odolinski, D. Odijk: Instantaneous BeiDou+GPS RTK positioning with high cut-off elevation angles, J. Geodesy **88**(4), 335–350 (2014)

25.101 J. Tegedor, O. Øvstedal: Triple carrier precise point positioning (PPP) using GPS L5, Survey Rev. **46**(337), 288–297 (2014)

25.102 P.J.G. Teunissen, D. Odijk, B. Zhang: PPP-RTK: Results of CORS network-based PPP with integer ambiguity resolution, J. Aeronaut. Astronaut. Aviat, Ser. A **42**(4), 223–230 (2010)

25.103 E. Schönemann: Analysis of GNSS Raw Observations in PPP Solutions, Ph.D. Thesis (TU Darmstadt, Darmstadt 2013)

25.104 H. Chen, W. Jiang, M. Ge, J. Wickert, H. Schuh: Efficient high-rate satellite clock estimation for PPP ambiguity resolution using carrier-ranges, Sensors **14**(12), 22300–22312 (2014)

25.105 O. Montenbruck, U. Hugentobler, R. Dach, P. Steigenberger, A. Hauschild: Apparent clock variations of the block IIF-1 (SVN-62) GPS satellite, GPS Solutions **16**(3), 303–313 (2012)

25.106 G. Wübbena, M. Schmitz, A. Bagg: PPP-RTK: Precise point positioning using state-space representation in RTK networks, Proc. ION GNSS 2005, Long Beach (ION, Virginia 2005) pp. 13–16

25.107 D. Laurichesse, F. Mercier: Integer ambiguity resolution on undifferenced GPS phase measurements and its application to PPP, Proc. ION GNSS 2007, Fort Worth (ION, Virginia 2007) pp. 839–848

25.108 L. Mervart, Z. Lukes, C. Rocken, T. Iwabuchi: Precise point positioning with ambiguity resolution in real-time, Proc. ION GNSS 2008, Savannah (ION, Virginia 2008) pp. 397–405

25.109 P. Collins: Isolating and estimating undifferenced GPS integer ambiguities, Proc. ION NTM 2008, San-Diego (ION, Virginia 2008) pp. 720–732

25.110 M. Ge, G. Gendt, M. Rotacher, C. Shi, J. Liu: Resolution of GPS carrier-phase ambiguities in precise point positioning (PPP) with daily observations, J. Geodesy **82**(7), 389–399 (2008)

25.111 W. Bertiger, S. Dessai, B. Haines, N. Harvey, A.W. Moore, S. Owen, P. Weiss: Single receiver phase ambiguity resolution with GPS data, J. Geodesy **84**(5), 3337 (2010)

25.112 J. Geng, F.N. Teferle, X. Meng, A.H. Dodson: Towards PPP-RTK: Ambiguity resolution in real-time precise point positioning, Adv. Space Res. **47**(10), 1664–1673 (2011)

25.113 A. Lannes, J.L. Prieur: Calibration of the clock-phase biases of GNSS networks: The closure-ambiguity approach, J. Geodesy **87**(8), 709–731 (2013)

25.114 P. Collins, S. Bisnath, F. Lahaye, P. Héroux: Undifferenced GPS ambiguity resolution using the decoupled clock model and ambiguity datum fixing, Navigation **57**(2), 123–135 (2010)

25.115 D. Laurichesse, F. Mercier, J.P. Berthias, P. Broca, L. Cerri: Integer ambiguity resolution on undifferenced GPS phase measurements and its application to PPP and satellite precise orbit determination, Navigation **56**(2), 135–149 (2009)

25.116 B. Zhang, P.J.G. Teunissen, D. Odijk: A novel undifferenced PPP-RTK concept, J. Navigation **64**(S1), 180–191 (2011)

25.117 J. Geng, C. Shi, M. Ge, A.H. Dodson, Y. Lou, Q. Zhao, J. Liu: Improving the estimation of fractional-cycle biases for ambiguity resolution in precise point positioning, J. Geodesy **86**(8), 579–589 (2013)

25.118 G. Blewitt: Fixed point theorems of GPS carrier-phase ambiguity resolution and their application to massive network processing: Ambizap, J. Geophys. Res. **113**(B12410), 1–12 (2008)

25.119 D. Odijk, P.J.G. Teunissen, B. Zhang: Single-frequency integer ambiguity resolution enabled GPS precise point positioning, J. Survey Eng. **138**(4), 193–202 (2012)

25.120 L. Mervart, C. Rocken, T. Twabuchi, Z. Lukes, M. Kanzaki: Precise point positioning with fast ambiguity resolution prerequisites, algorithms and performance, Proc. ION GNSS 2013, Nashville (ION, Virginia 2013) pp. 1176–1185

25.121 X. Li, M. Ge, H. Zhang, J. Wickert: A method for improving uncalibrated phase delay estimation and

ambiguity fixing in real-time precise point positioning, J. Geodesy **87**(5), 405–416 (2013)
25.122 S. Banville, P. Collins, P. Héroux, P. Tétreault, P.F. Lahaye: Precise cooperative positioning: A case study in Canada, Proc. ION GNSS 2014, Tampa (ION, Virginia 2014) pp. 2503–2511
25.123 P. Collins, F. Lahaye, S. Bisnath: External ionospheric constraints for improved PPP-AR initialisation and a generalised local augmentation concept, Proc. ION GNSS 2012, Nashville (ION, Virginia 2012) pp. 3055–3065
25.124 J. Geng, Y. Bock: Triple-frequency GPS precise point positioning with rapid ambiguity resolution, J. Geodesy **87**(5), 449–460 (2013)
25.125 L. Pan, C. Cai, R. Santerre, J. Zhu: Combined GPS/GLONASS precise point positioning with fixed GPS ambiguities, Sensors **14**, 17530–17547 (2014)
25.126 D. Odijk, B. Zhang, P.J.G. Teunissen: Multi-GNSS PPP and PPP-RTK: Some GPS+BDS results in Australia, Proc. CSNC (2015) Vol. II, Xi'an, ed. by J. Sun, J. Liu, S. Fan, X. Lu (Springer, Berlin 2015) pp. 613–623
25.127 L. Qu, Q. Zhao, J. Guo, G. Wang, X. Guo, Q. Zhang, K. Jiang, L. Luo: BDS/GNSS real-time kinematic precise point positioning with un-differenced ambiguity resolution, Proc. CSNC, Vol. III (2015), Xi'an, ed. by J. Sun, J. Liu, S. Fan, X. Lu (Springer, Berlin 2015) pp. 13–29
25.128 G. Weber, D. Dettmering, H. Gebhard, R. Kalafus: Networked transport of RTCM via internet protocol (Ntrip) – IP-streaming for real-time GNSS applications, Proc. ION GPS 2005, Long Beach (ION, Virginia 2005) pp. 2243–2247
25.129 The Precise Point Positioning Center (Univ. New-Brunswick, Frederiction 2015), http://gge.unb.ca/Resources/PPP/Purpose.html
25.130 P. Héroux, J. Kouba: GPS precise point positioning using IGS orbit products, Phys. Chem. Earth (A) **26**(6–8), 573–578 (2001)
25.131 H. Bock, R. Dach, A. Jäggi, G. Beutler: High-rate GPS clock corrections from CODE: Support of 1 Hz applications, J. Geodesy **83**(11), 1083–1094 (2009)
25.132 S.H. Byun, Y.E. Bar-Sever: A new type of troposphere zenith path delay product of the international GNSS service, J. Geodesy **83**(3/4), 1–7 (2009)
25.133 G. Gendt: IGS combination of tropospheric estimates – Experience from pilot experiment, Proc. Anal. Center Workshop (1998) Darmstadt, ed. by J.M. Dow, J. Kouba, T. Springer (IGS, Pasadena 1998) pp. 205–216
25.134 K. Senior, P. Koppang, D. Matsakis, J. Ray: Developing an IGS time scale, Proc. IEEE Freq. Contr. Symp. 2001, Seattle (IEEE, Washington 2001) pp. 211–218
25.135 J. Dow, R.E. Neilan, G. Gendt: The International GPS Service (IGS): Celebrating the 10th anniversary and looking to the next decade, Adv. Space Res. **36**, 320–326 (2005)